The distinctive germinal center phase of IgE+ B lymphocytes limits their contribution to the classical memory response

Jin-Shu He,[1] Michael Meyer-Hermann,[2] Deng Xiangying,[1] Lim Yok Zuan,[1] Leigh Ann Jones,[1] Lakshmi Ramakrishna,[1] Victor C. de Vries,[1] Jayashree Dolpady,[3] Hoi Aina,[1] Sabrina Joseph,[1] Sriram Narayanan,[1] Sharrada Subramaniam,[1] Manoj Puthia,[1] Glenn Wong,[1] Huizhong Xiong,[3] Michael Poidinger,[1] Joseph F. Urban,[4] Juan J. Lafaille,[3] and Maria A. Curotto de Lafaille[1,3]

[1]Singapore Immunology Network (SIgN), Agency for Science, Technology and Research (A*STAR), Singapore 138648
[2]Department of Systems Immunology, Helmholtz Centre for Infection Research and Department of Life Sciences, Technische Universität Braunschweig, D-38124 Braunschweig, Germany
[3]The Kimmel Center for Biology and Medicine of the Skirball Institute and Department of Pathology, New York University School of Medicine, New York, NY 10016
[4]Beltsville Human Nutrition Research Center, Agricultural Research Service, United States Department of Agriculture, Beltsville, MD 20705

The mechanisms involved in the maintenance of memory IgE responses are poorly understood, and the role played by germinal center (GC) IgE+ cells in memory responses is particularly unclear. IgE+ B cell differentiation is characterized by a transient GC phase, a bias toward the plasma cell (PC) fate, and dependence on sequential switching for the production of high-affinity IgE. We show here that IgE+ GC B cells are unfit to undergo the conventional GC differentiation program due to impaired B cell receptor function and increased apoptosis. IgE+ GC cells fail to populate the GC light zone and are unable to contribute to the memory and long-lived PC compartments. Furthermore, we demonstrate that direct and sequential switching are linked to distinct B cell differentiation fates: direct switching generates IgE+ GC cells, whereas sequential switching gives rise to IgE+ PCs. We propose a comprehensive model for the generation and memory of IgE responses.

CORRESPONDENCE
Maria A. Curotto de Lafaille:
maria_lafaille@immunol.a-star.edu.sg

Abbreviations used: CSR, class switch recombination; DZ, dark zone; FDC, follicular DC; GC, germinal center; GSEA, Gene set enrichment analysis; LZ, light zone; mLN, mesenteric LN; PC, plasma cell; Tfh, T follicular helper cell.

IgE antibodies are critical mediators of allergic reactions (Gould and Sutton, 2008). Cross-linking of IgE molecules bound to high affinity FcεRI receptors on mast cells and basophils leads to the rapid release of potent proinflammatory molecules (Kinet, 1999; Galli and Tsai, 2012). In spite of its pathological potential, IgE exhibits the lowest serum concentration and the shortest half-life of all the antibody isotypes (Vieira and Rajewsky, 1988; Gould and Sutton, 2008). The low frequency of IgE-producing cells makes their study particularly challenging. Using mouse models of high IgE responses (Katona et al., 1988; Curotto de Lafaille et al., 2001), we discovered that IgE-producing cells develop via a unique differentiation pathway that occurs during the germinal center (GC) phase of T cell–dependent responses and yet favors the production of plasma cells (PCs; Erazo et al., 2007; Yang et al., 2012). In our early studies a GC IgE+ population was not clearly detectable, but the IgE antibodies produced were observed to have undergone affinity maturation, indicating a GC history for IgE+ PC. We proposed at the time that high affinity IgE originated from the sequential switching of high affinity IgG1 cells, and hence we speculated that classical IgE+ memory cells may be absent in mice (Erazo et al., 2007; Curotto de Lafaille and Lafaille, 2010).

Sequential switching of IgG cells to IgE was first discovered by the identification of switch(S)γ region footprints in the Sμ-Sε DNA region of IgE genes (Matsuoka et al., 1990; Yoshida et al., 1990; Jabara et al., 1993; Mandler et al., 1993;

The Rockefeller University Press $30.00
J. Exp. Med. 2013 Vol. 210 No. 12 2755-2771
www.jem.org/cgi/doi/10.1084/jem.20131539

The Journal of Experimental Medicine

Zhang et al., 1994; Baskin et al., 1997), but the biological significance of this finding was at that time unknown. Sequential switching in mice entails two recombination events, Sμ→Sγ1 and SμSγ1→Sε, that may be either continuous or temporally separate events. The latter scenario allows for the existence of an intermediate IgG1 cellular phase in which affinity maturation can occur in GCs. Indeed, stimulation of IgG1 cells in the presence of IL-4 either in vivo or in vitro resulted in the production of IgE antibodies (Erazo et al., 2007; Wesemann et al., 2012). Importantly, mice deficient in class switching to IgG1 due to a mutation in the Iγ1 exon (Lorenz et al., 1995) were unable to produce high affinity IgE antibodies (Xiong et al., 2012a,b), indicating that sequential switching is essential for the formation of high affinity IgE.

The recent development of fluorescent reporter mice for IgE has facilitated the identification of IgE GC cells (Talay et al., 2012; Yang et al., 2012). However, the in vivo phenotype and role of IgE GC cells in supporting IgE responses and its relationship with the sequential switching process remain unclear (Lafaille et al., 2012; Xiong et al., 2012a).

In the current study, we used a new reporter mouse for class switch recombination (CSR) to IgE, improved methods to functionally study IgE B cells ex vivo and in vivo, and in silico modeling to analyze the origin, functional properties, and population dynamics of IgE GC cells and PC. We show that IgE GC cells are unfit to undergo the conventional GC differentiation program and instead undergo apoptosis at a high rate. This "failure to thrive" of IgE GC cells greatly limits their contribution to the memory pool and high affinity PC compartment. Furthermore, we show that the two types of rearrangement to IgE are associated with distinct B cell differentiation fates. Direct Sμ-Sε rearrangements generate IgE GC cells, whereas sequential switching of IgG1 cells gives rise to IgE PC.

RESULTS

Expression of GFP in CεGFP mice reports all CSR to Cε

To track immunoglobulin gene CSR to IgE in vivo and in vitro, we generated the CεGFP reporter mice. These mice carry an *IRES-GFP* cassette insertion in the 3′ untranslated region of the membrane-encoding Cε gene that preserves native polyadenylation signals (Fig. 1 A and Fig. S1 A). In vitro stimulation of naive splenocytes from CεGFP mice with either LPS or anti-CD40 in the presence of IL-4 led to the appearance of GFP$^+$ cells concurrently with production of IgE antibodies, whereas LPS or anti-CD40 stimulation alone did not (Fig. S1, B and C).

To assess GFP expression in vivo, we infected CεGFP BALB/c mice with the parasite *Nippostrongylus brasiliensis*, a known inducer of Th2 responses and IgE production (Urban et al., 1992). Parasite infection resulted in the expected appearance of IgE$^+$GFP$^+$ cells and also elicited a population of IgG1$^+$GFP$^+$ cells in LNs (Fig. 1 B). All GFP$^+$ cells expressed CD95 (Fig. 1 B). Only IgE$^+$ cells expressed the mature IgE transcript, whereas the post-switched Cε transcript was expressed by both IgE$^+$GFP$^+$ cells and IgG1$^+$GFP$^+$ cells, but not by IgG1$^+$GFP$^-$ cells (Fig. 1 C). It is well established that CSR can occur in both IgH alleles (Rabbitts et al., 1980; Siebenkotten et al., 1992; Erazo et al., 2007); thus, the expression of both GFP and switched Cε transcript in IgG1$^+$GFP$^+$ indicates that these cells underwent recombination to Sε in the nonproductive IgH allele (Fig. 1 D). These data demonstrate that GFP expression in the novel IgE reporter CεGFP mice uniquely identifies all events of CSR to Cε.

Marked differences in population dynamics of IgE$^+$ and IgG1$^+$ GC cells

We next characterized IgG1$^+$ and IgE$^+$ cells in mesenteric LN (mLN) from CεGFP at 10 d after infection with *N. brasiliensis*. IgE$^+$ and IgG1$^+$ cells could each be separated into a B220^{lo}CD138/Syndecan-1$^+$ PC population that expressed *Prdm1*, *Irf4*, and *Xbp1*, and a B220$^+$CD138$^-$ GC population that instead expressed *Bcl6* and *Aicda* (Fig. 1, E and F). Gene array analysis revealed very similar gene expression patterns within the IgE$^+$ and IgG1$^+$ (IgG1$^+$GFP$^+$ and IgG1$^+$GFP$^-$) GC cells (Fig. 1 G). IgE$^+$ GC cells expressed lower levels of Ig than did IgE$^+$ PC cells (Fig. 1 H), whereas IgG1$^+$ GC cells (both GFP$^+$ and GFP$^-$) expressed higher Ig levels than did their IgG1$^+$ PC counterparts (Fig. 1 H), as previously reported (Erazo et al., 2007; Xiong et al., 2012b; Yang et al., 2012). The predominance of the PC in the IgE$^+$ population (Erazo et al., 2007) was evident at 10 d after infection, at which point IgE$^+$GFP$^+$ PC comprised ∼50% of the total IgE$^+$GFP$^+$ cells in mLN, while IgG1$^+$ GC cells greatly outnumbered IgG1$^+$ PC (Fig. 1 E).

We next sought to track cells carrying rearrangements to Cε during infection with *N. brasiliensis*, which included IgE cells, as well as IgG1 cells expressing GFP. Because the mice were heterozygous for the CεGFP insertion, GFP$^+$ cells comprised approximately half of the total cells carrying Sε rearrangements. Due to the low level of IgE surface expression, IgE$^+$GFP$^-$ GC cells could not be reliably tracked. IgG1$^+$GFP$^-$ and IgG1$^+$GFP$^+$ GC cells displayed similar kinetics, albeit very different frequency. IgE$^+$GFP$^+$ GC expanded quickly up to 13 d, similarly to IgG1$^+$ GC cells, but declined very rapidly thereafter (Fig. 2 A). The similar frequencies of IgE$^+$GFP$^+$ and IgG1$^+$GFP$^+$ GC cells up to 13 d after infection suggests that switching to IgE occurred at comparable rates in both the productive and nonproductive IgH alleles (Fig. 2 A). As the frequency of IgE$^+$ GC cells began to decline from day 13 onward, the IgG1$^+$GFP$^+$ cells began to outnumber the IgE$^+$GFP$^+$ population. During secondary infection, the increase in IgE$^+$ GC cell frequency was also transient whereas IgG1$^+$ GC cell numbers were more stable (Fig. 2 A).

The frequency of IgE$^+$ PC (both GFP$^+$ and GFP$^-$) at 10 d after infection was similar to that of IgE$^+$GFP$^+$ GC cells, but the IgE$^+$ PC population decreased rapidly thereafter and their decline preceded the loss of IgE$^+$GFP$^+$ GC cells (Fig. 2, A and B). These data are inconsistent with the previously proposed model in which the primary cause of declining IgE$^+$ GC cell numbers was attributed to be their differentiation into PC (Yang et al., 2012). After secondary infection

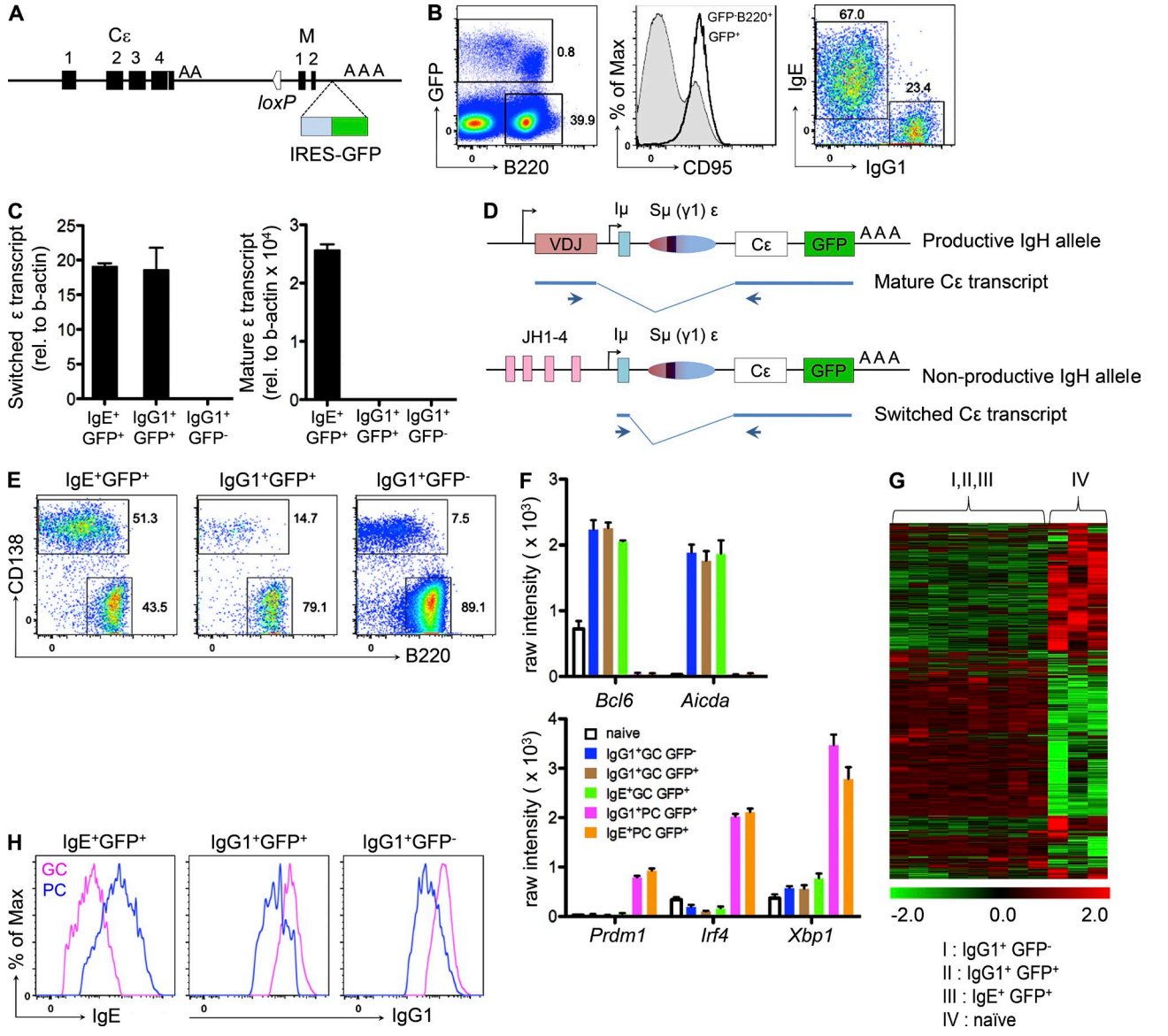

Figure 1. CεGFP mice efficiently report all CSR to Cε. (A) Schematic representation of CεGFP KI integration into the *IgH Cε* locus. (B–H) CεGFP BALB/c mice were infected with *N. brasiliensis* and mLNs were collected 10 d later for analysis by flow cytometry and sorting. (B) Left: frequency of GFP$^+$ cells among total lymphocytes; middle: CD95 expression on GFP$^+$ cells and GFP$^-$B220$^+$ cells; right: frequency of IgE$^+$ and IgG1$^+$ cells within the gated GFP$^+$ population. (C) QPCR analysis of Cε switched (left) and mature (right) transcripts in sorted IgE$^+$GFP$^+$, IgG1$^+$GFP$^+$, and IgG1$^+$GFP$^-$B220$^+$ cells. Error bars indicate SD of duplicated samples. Data are representative of two independent experiments with $n = 3$ mice pooled per experiment. (D) Schematic representation of mature Cε and switched Cε transcripts driving *GFP* expression from the productive and nonproductive *IgH* alleles. (E) Numbers indicate frequency of B220^{lo}CD138$^+$ PC and B220$^+$CD138$^-$ GC cells among gated IgE$^+$GFP$^+$, IgG1$^+$GFP$^+$, and IgG$^+$GFP$^-$ cells. (F and G) IgE$^+$ and IgG1$^+$ LN cells from day 10 *N. brasiliensis* CεGFP BALB/c-infected mice were sorted into B220^{lo}CD138$^+$ PC and B220$^+$CD138$^-$ GC cell populations. Naive B220$^+$FAS$^-$IgG1$^-$IgE$^-$ cells were sorted as a control reference population. Gene expression was analyzed using the Affymetrix Mouse Exon 1.0 ST Array. (F) Graphs showed hybridization intensities for GC genes *Bcl6* and *Aicda* and for PC genes *Prdm1*, *Irf4*, and *Xbp1* within the sorted populations. Error bars indicate SEM of $n = 3$–4 samples per group. (G) Heat-map representation of the 8,120 probes differentially expressed in at least one comparison between group IV and groups I, II, or III in the GC array. Probes have been z-score normalized. Similar patterns of gene expression were observed across groups I, II, and III, but not in group IV. (H) Membrane immunoglobulin levels on gated IgE$^+$GFP$^+$, IgG1$^+$GFP$^+$, and IgG$^+$GFP$^-$ GC and PC cells. Data shown are representative of at least five experiments (B, E, and H), $n = 3$–5 mice per experiment.

IgE$^+$ and IgG1$^+$ PC frequency in LN transiently increased (Fig. 2 B). IgE$^+$ PC and IgG1$^+$ PC cells were detected in the BM at 21 d after primary infection and also after secondary infection (Fig. 2 C).

These kinetic analyses identified two distinct phases of the primary GC B cell response in *N. brasiliensis*–infected mice: an initial infective phase that is characterized by the rapid generation and expansion of IgE$^+$ and IgG1$^+$ GC cells, followed by

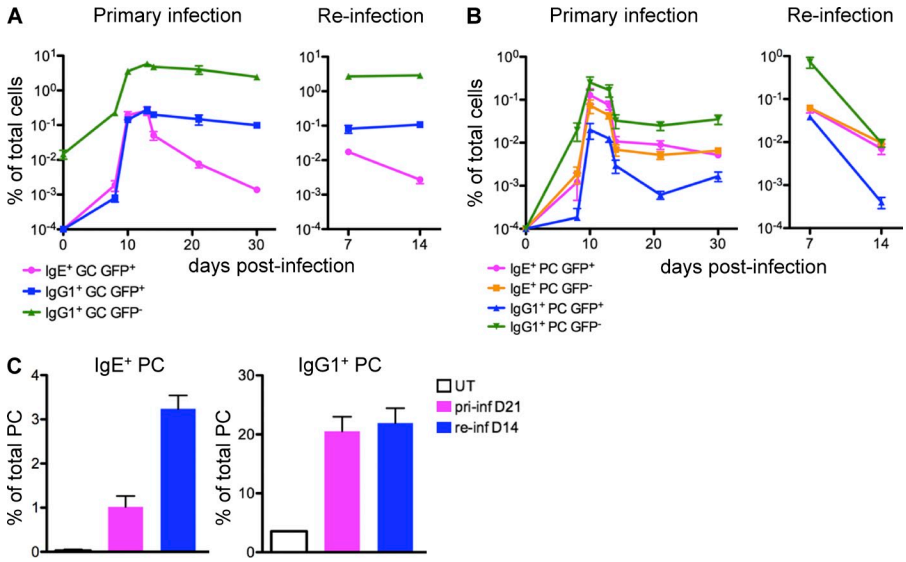

Figure 2. Population dynamics of IgE$^+$ and IgG1$^+$ cells during infection with *N. brasiliensis*. CεGFP BALB/c mice were infected with *N. brasiliensis* and a group of mice were reinfected 40 d later. (A and B) mLN were collected on days 8, 10, 13, 14, 21, and 30 after primary infection, and on days 7 and 14 after reinfection. (A and B) Kinetics of IgE$^+$GFP$^+$, IgG1$^+$GFP$^+$, and IgG1$^+$GFP$^-$ GC cells (A) and IgE$^+$GFP$^+$, IgE$^+$GFP$^-$, IgG1$^+$GFP$^+$, and IgG1$^+$GFP$^-$ PCs (B) during primary and secondary *N. brasiliensis* infection. The frequencies of each cell population are given as proportion of total DAPI$^-$ viable cells. (C) Frequency of BM IgE$^+$ PC and IgG1$^+$ PC on day 21 of primary infection (pri-inf) and on day 14 of reinfection (re-inf) with *N. brasiliensis*. UT, untreated mice. n = 3–6 mice per time point from two independent experiments were analyzed (A–C). Error bars indicate SEM.

a second phase commencing after worm expulsion on day 11 after infection (Camberis et al., 2003), at which time IgE$^+$ GC steeply decline and IgG1$^+$ GC cells persist.

Functional deficiency in B cell receptor expression and signaling in IgE GC cells

We next hypothesized that a deficiency in BCR expression and/or signaling could underlie the surprisingly rapid decline of IgE$^+$ GC cells in parasite-infected CεGFP mice. To directly compare BCR expression between IgE$^+$ and IgG1$^+$ cells, we next studied these populations in TBmc mice (Curotto de Lafaille et al., 2001), in which all B cells are specific for the HA peptide. This enabled us to use the same peptide antigen to stain the BCR in both IgG1$^+$and IgE$^+$ cells. BCR levels were quantified in mLN cells isolated on day 12 after immunization by staining with the peptide HA and with antibodies against IgE and IgG1. Mutations in V(D)J genes are rare at this time point in TBmc mice (Erazo et al., 2007); hence, HA binding was neither compromised, nor did it interfere with the binding of isotype-specific antibodies (Fig. 3, A and B). Analysis of HA binding level (MFI) demonstrated that surface immunoglobulin levels in IgE$^+$ GC cells were three- to fourfold lower than in IgG1$^+$ GC cells (Fig. 3, C and D). In contrast, IgE$^+$ PCs expressed three- to fourfold higher levels of membrane immunoglobulin than did IgG1$^+$ cells (Fig. 3 D).

We next investigated the correlation of surface BCR expression with transcript levels for total Ig, membrane-bound Ig, and secreted Ig (Fig. 3 E). We detected comparable levels of mature steady-state transcripts in both IgE$^+$ and IgG1$^+$ GC cells, as well as in both IgE$^+$ PC and IgG1$^+$ PC, although total transcript expression level was >100-fold higher in PC cells compared with GC cells (Fig. 3 F). IgE$^+$ GC cells produced atypically high levels of secreted IgE transcripts but low levels of IgE membrane transcripts (Fig. 3, G and H), as has previously also been described for IgE$^+$B220$^+$ cells (Karnowski et al., 2006). In addition, membrane IgE transcripts were up-regulated in IgE$^+$ PC compared with IgE$^+$ GC cells, whereas the reverse was the case for IgG1$^+$ cells (Fig. 3 H), consistent with our earlier flow cytometry data (Fig. 1 H).

BCR expression and signaling are essential for the survival of mature B cells (Lam et al., 1997; Kraus et al., 2004), and both BCR/Ag-internalization and BCR signaling are thought to be necessary for effective selection and survival in the GC (Tarlinton and Smith, 2000; Hou et al., 2006; Vascotto et al., 2007; Victora and Nussenzweig, 2012). We therefore investigated whether the rapid decline of IgE$^+$ GC cells in CεGFP mice could be due to impaired BCR signaling in this population. A previous report identified that IgM$^+$ GC cells exhibit impaired BCR signaling (except during G2/M) due to a high level of phosphatase activity (Khalil et al., 2012), and similarly, we observed that switched IgG1$^+$ and IgE$^+$ GC cells from TBmc mice responded poorly to BCR cross-linking (Fig. 4 A). Treatment of GC cells with increasing concentrations of the phosphatase inhibitor H_2O_2 led to a dose-dependent phosphorylation of proximal signaling molecules Syk and Blnk (Fig. 4, B and C). Phosphorylation of Erk1/2 occurs downstream of BCR and CD40 signaling, and high levels of p-Erk1/2 expression were induced even at the lowest H_2O_2 concentration (Fig. 4, B and C). Interestingly, when subjected to suboptimal stimulation, IgE$^+$ GC cells exhibited far lower levels of p-Syk and p-Blnk than did IgG1$^+$ GC cells (Fig. 4, B and C), consistent with a reduced number of BCR signaling complexes in IgE$^+$ cells. It is unlikely that this reflects inherent differences in phosphatase activity because both the SHP-1 and SHIP-1 phosphatases that regulate BCR signaling (Cyster and Goodnow, 1995; Pani et al., 1995; Liu et al., 1998; Okada et al., 1998) were expressed at similar transcriptional levels in IgE$^+$ and IgG1$^+$ GC cells (not depicted).

In addition to the BCR levels, we quantified the expression of other surface receptors important for antigen presentation and costimulation, such as MHC II, CD19, CD40,

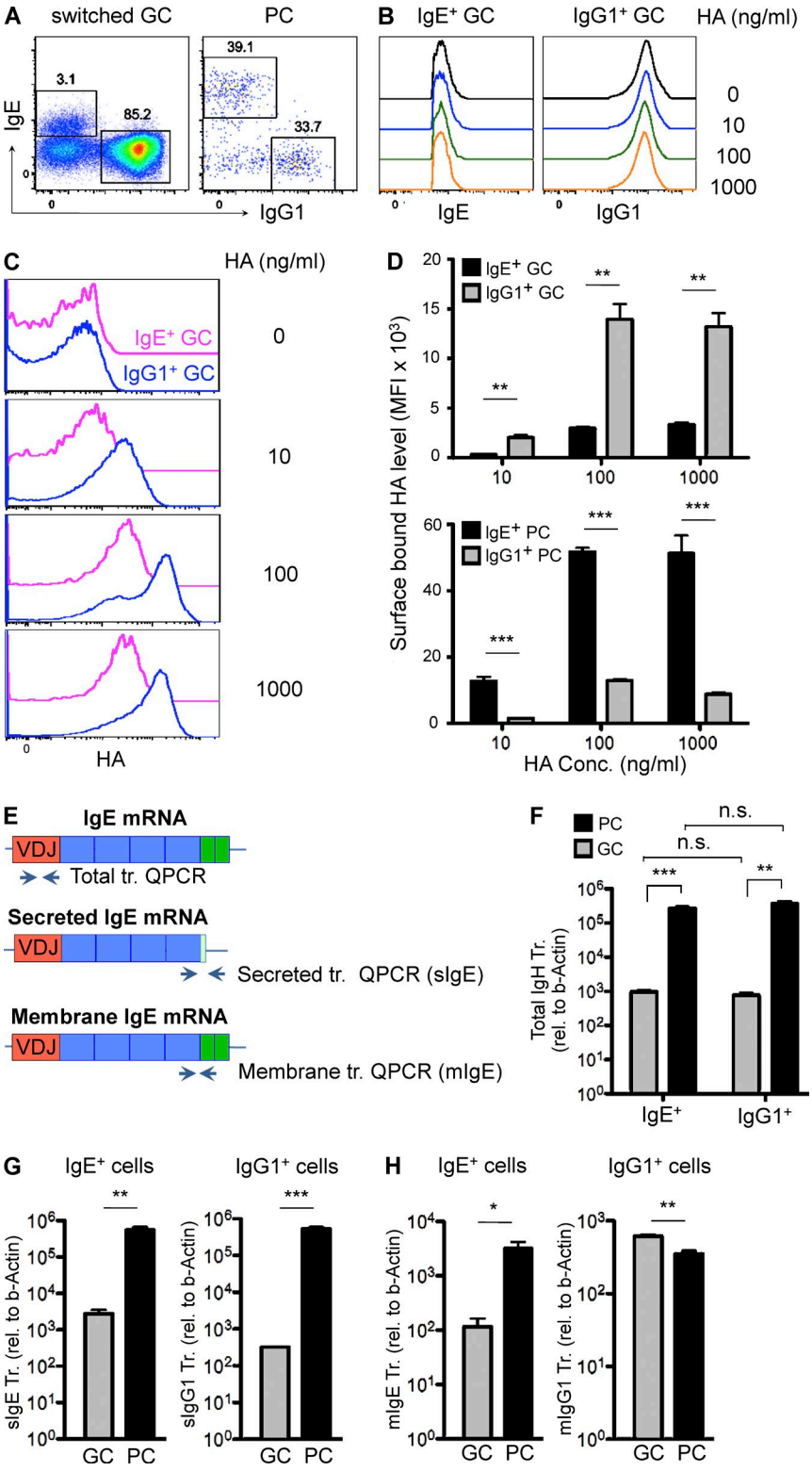

Figure 3. Dysregulated expression of membrane and secreted immunoglobulin in IgE+ cells. (A–D) TBmc mice were immunized with OVA-HA and the mLNs were harvested 12 d later. Cells were incubated with 0–1,000 ng/ml of labeled HA peptide, along with antibodies. (A) Dot plots show the frequencies of IgE+ and IgG1+ cells among the gated IgD−IgM−B220+CD138− switched GC cells and among CD138+B220lo PC populations. (B) Binding competition between HA peptide and antibodies against membrane immunoglobulin was examined by flow cytometry. Histograms show fluorescence intensity of IgE and IgG1 staining in GC cells costained with increasing concentrations of HA. (C) Histograms show levels of surface-bound HA on IgE+ and IgG1+ GC cells. (D) MFI of bound HA on GC populations (top) and on PC populations (bottom) was determined at different peptide concentrations by subtracting the MFI value of the HA unstained control samples. (E) QPCR primer locations for total IgE, membrane-bound IgE, and secreted IgE transcripts (tr.). (F–H) CεGFP TBmc mice were immunized with OVA-PEP1 and the mLN were harvested 12 d later. (F) QPCR analysis of total VDJ transcript levels in purified IgE+ and IgG1+ GC cells and IgE+ and IgG1+ PC. (G and H) QPCR analysis of secreted and membrane Cε transcripts, and secreted and membrane Cγ1 transcripts in IgE+ and IgG1+ GC cells and in IgE+ and IgG1+ PC. Error bars indicate SEM of $n = 3$ mice (D and F–H). *, $P < 0.05$; **, $P < 0.01$; ***, $P < 0.001$. Data are representative of two independent experiments (A–D and F–H).

CD80, LIGHTR, CD21/CD35, ICOSL, and OX40L. We found that expression of the surface C3d receptor CD21/CD35, and of ICOSL and OX40L, were significantly reduced in IgE+ GC cells compared with IgG1+ GC cells (Fig. 5, A and B).

In sum, we demonstrated marked differences in the regulation of membrane and secreted Ig expression between IgG1+ and IgE+ cells, and in particular, that IgE+ GC cells exhibit decreased BCR expression and reduced proximal signaling upon phosphatase inhibition.

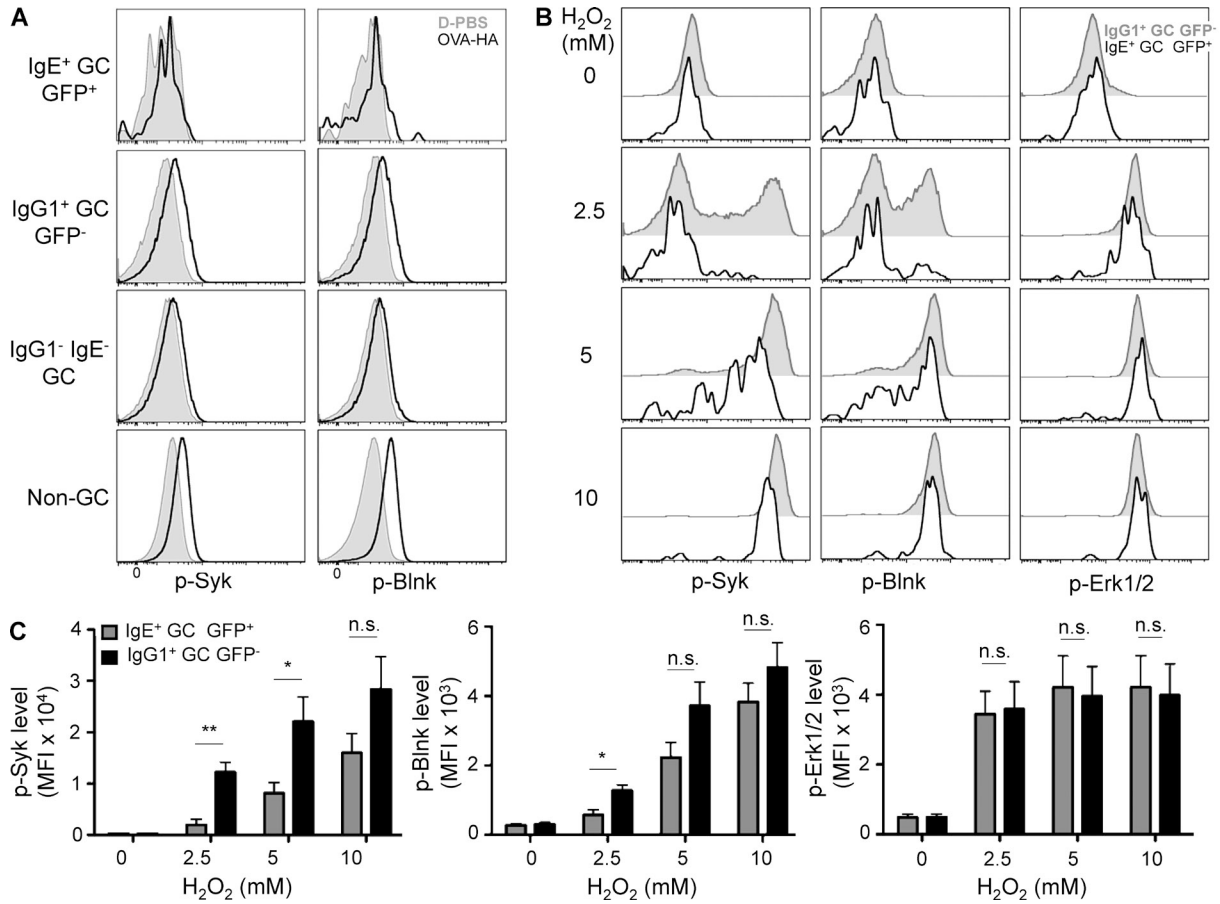

Figure 4. BCR signaling is reduced in IgE+ GC cells compared with IgG1+ GC cells upon ex vivo stimulation. (A) Single cell suspensions of mLN from OVA-HA immunized CεGFP TBmc mice were treated with D-PBS or stimulated ex vivo with 10 µg/ml OVA-HA for 5 min. Levels of p-Syk and p-Blnk expression were determined by flow cytometry within gated populations of IgE+GFP+ cells, IgG1+GFP+, and IgG1−IgE− GC cells, and B220+CD95− non-GC cells (black line histograms). Gray filled histograms correspond to D-PBS–treated controls. Data are representative of two independent experiments (n = 9 mice pooled per experiment). (B) Cells from immunized CεGFP TBmc mice were untreated or stimulated with increasing concentrations of H_2O_2 for 10 min. Histograms show p-Syk, p-Blnk, and p-Erk1/2 expression levels in gated IgE+GFP+ GC cells (black line) and in IgG1+GFP− GC cells (solid gray). Data are representative of nine independent experiments (n = 6–9 mice pooled per experiment). (C) Quantification of p-Syk, p-Blnk and p-Erk1/2 levels (MFI) in H_2O_2-stimulated IgE+GFP+ and IgG1+GFP− GC cells from four independent experiments (n = 6–9 mice pooled per experiment). Error bars represent SEM. *, P < 0.05; **, P < 0.01.

Increased dark zone (DZ) apoptosis and reduced light zone (LZ) frequency suggest decreased DZ to LZ output of IgE+ GC cells

GCs are anatomically and functionally separated into two distinct zones: a DZ, wherein cell proliferation and somatic hypermutation occur, and an LZ, where GC cells undergo selection via interactions with follicular DCs (FDCs) and T follicular helper cells (Tfh cells; Kelsoe, 1996; Victora and Nussenzweig, 2012). The LZ and DZ environments are maintained by differential expression of the chemokines CXCL12 (DZ) and CXCL13 (LZ), and GC B cells in these different zones can be distinguished by the differential expression of CXCR4 and CD86/CD83 (Allen et al., 2004; Victora et al., 2010).

Intriguingly, analysis of the LZ/DZ distribution of IgE+ and IgG1+ cells demonstrated a threefold reduction in the frequency of IgE+ cells exhibiting the characteristic CXCR4−CD86+ LZ phenotype compared with IgG1+ cells (Fig. 6, A and B). Differentially expressed LZ and DZ gene sets were then generated by comparison of the LZ and DZ gene expression profiles of IgG1+ cells (Table S2). GeneGo pathway analysis of LZ and DZ genes yielded comparable results to previously reported data (Victora et al., 2010, 2012), although we did observe a novel increase in mitochondria redox activity in DZ cells (Table S2). This pathway was found to be specifically up-regulated in GC cells among all B lymphocyte populations when compared in Immgen (Heng and Painter, 2008). Gene set enrichment analysis (GSEA) of the LZ and DZ gene signatures of total IgE+ and IgG1+ GC cells (Fig. 6 C and Table S2) revealed enrichment of the DZ gene signature among IgE+ cells (Fig. 6 C), which was consistent with our earlier flow cytometry data. BrdU incorporation identified a higher frequency of proliferating cells in the total IgE+ GC population than in total IgG1+ GC cells, reflecting the low LZ component of IgE+ GC cells (Fig. 6 D).

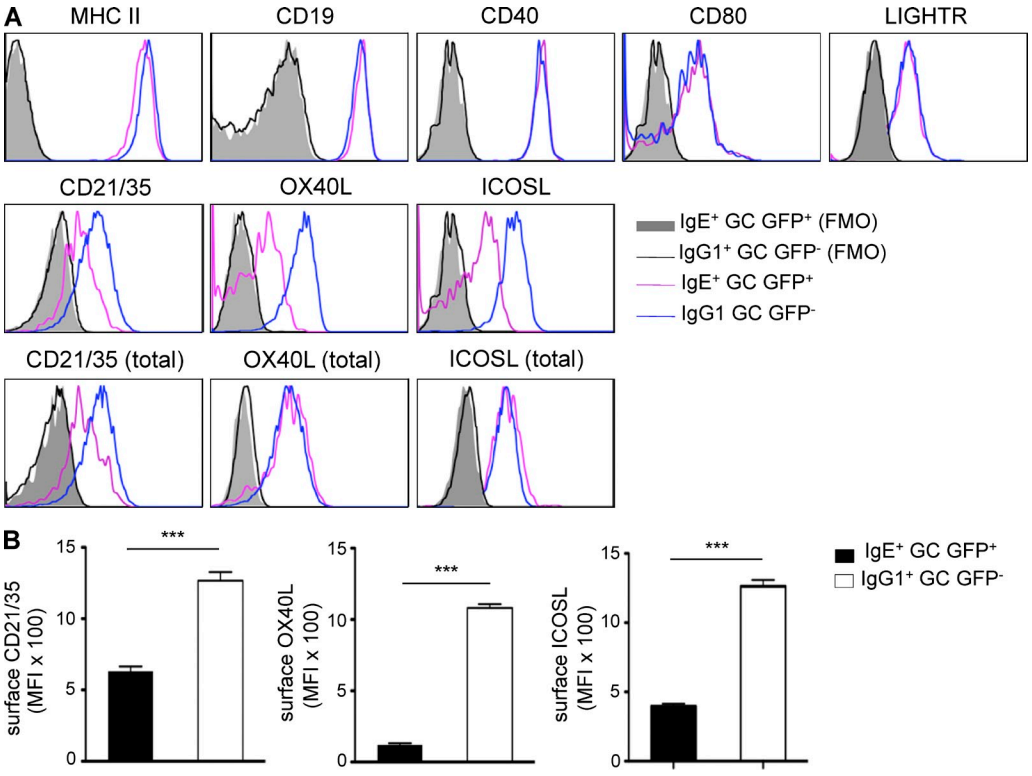

Figure 5. Decreased expression of costimulatory molecules on IgE+ GC cells. CεGFP BALB/c mice were infected with *N. brasiliensis* and mLN cells were harvested and analyzed 10 d later. (A) Flow cytometry analysis of MHC II, CD19, CD40, CD80, LIGHTR, CD21/35, OX40L, and ICOSL surface expression, and assessment of total (surface and intracellular) expression of CD21/35, OX40L, and ICOSL in gated IgE+GFP+ and IgG1+GFP− GC cells (FMO = Fluorescence Minus One control). (B) Quantification of surface expression levels (MFI) of CD21/35, OX40L, and ICOSL on gated IgE+GFP+ and IgG1+GFP− GC cells. Error bars indicate SEM of $n = 5$ mice. ***, $P < 0.001$. Data are representative of three independent experiments (A and B).

In addition to their low LZ frequency, IgE+ cells did not display up-regulation of BCR expression in the LZ relative to their counterparts in the DZ, whereas BCR levels among IgG1+ cells were ∼40% higher in LZ cells than in DZ cells (Fig. 6 E). These differences in distribution and DZ/LZ BCR expression were also evident in GC sections stained with antibodies against IgE/IgG1 and with anti-CD35 to identify FDC (Fig. 6 F). As previously reported (Erazo et al., 2007), brighter staining of IgG1+ cells was observed in the LZ of the GC, consistent with higher BCR expression in IgG1+ LZ cells than in the IgG1+ DZ cells. Most IgE+ GC cells appeared to be located in the DZ, reflecting the increased frequency of these cells in the DZ.

Because low expression of BCR and related costimulatory molecules may impair the selection and survival of GC cells, we next investigated whether IgE+ cells undergo apoptosis at a higher rate than do IgG1+ cells. Analysis of total Caspase activity among these populations (Fig. 6, G and H), together with assessment of activated Caspase-3 levels (not depicted), consistently indicated a two- to threefold higher incidence of apoptosis among IgE+ GC cells compared with IgG1+ GC cells (Fig. 6 H). Unexpectedly, the majority of IgE+ apoptotic cells (68%) accumulated in the DZ, whereas the majority of IgG1+ apoptotic cells (65%) were located in the LZ (Fig. 6, I and J).

The distribution of LZ and DZ B cells is determined by GC dynamics of cell proliferation, selection, apoptosis, differentiation, and intra-zonal migration (Victora et al., 2010; Meyer-Hermann et al., 2012). To determine the best-fit hypothesis for the IgE DZ/LZ distribution identified here, we next developed a mathematical model of CSR and IgE+ GC B cell properties using previously defined parameters for GC dynamics (including cell migration, division, selection, zonal exit, and antibody production; Meyer-Hermann et al., 2006, 2012; Figge et al., 2008; Garin et al., 2010; Zhang et al., 2013). This model also incorporated new parameters for IgM+ GC population kinetics, probability of CSR to IgE and IgG1, and immunoglobulin isotype-specific BCR expression.

Based on the reduced BCR expression of IgE+ GC B cells, two non–mutually exclusive scenarios were considered in silico. In the first scenario, IgE+ GC cells were less competitive than IgG1+ GC cells for antigen capture and were thus impaired in their ability to interact with Tfh cells and undergo selection in the LZ. Inefficient selection of IgE+ GC cells in the LZ was tested by reducing the probability of antigen uptake by IgE GC cells to <0.3 in the in silico model (based on BCR expression level among IgE+ cells being only 30% of that observed in IgG1+ GC, Fig. 3 D). However, this inefficient selection process was not sufficient to reproduce the DZ/LZ ratio of IgE+ cells observed in the wet laboratory (Fig. 6 K). In contrast, in the

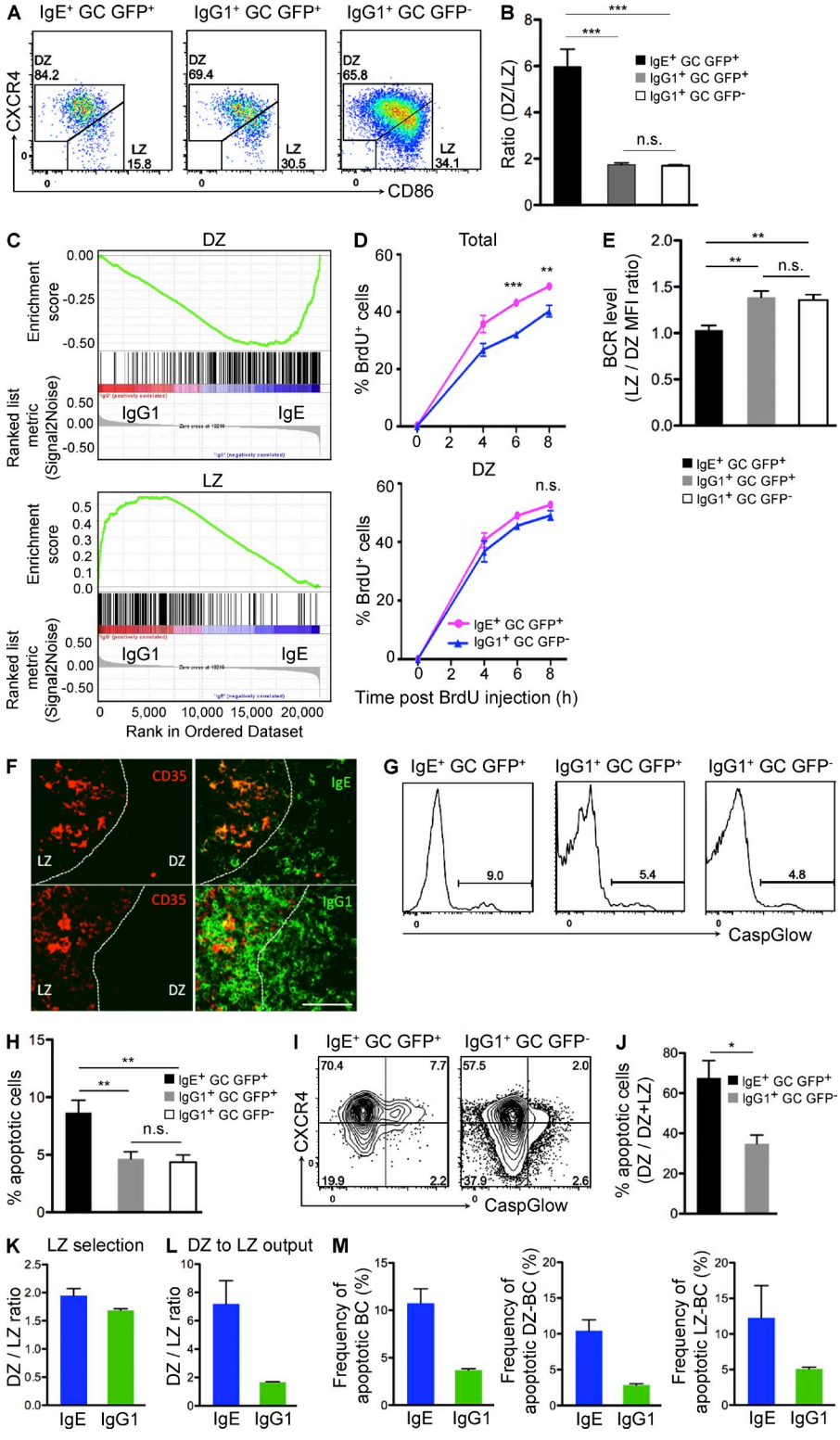

Figure 6. Altered LZ/DZ distribution and increased apoptosis of IgE+ GC cells compared with IgG1+ GC cells. Single cell suspensions were prepared from the mLN of CεGFP BALB/c mice on day 10 of infection with *N. brasiliensis*. (A) Dot plots show the DZ and LZ phenotypes among IgE+GFP+, IgG1+GFP+, and IgG1+GFP− GC cells. CXCR4 and CD86 were used as markers to discriminate GC LZ (CD86hiCXCR4lo) and DZ (CD86loCXCR4hi) cells. (B) Quantification of DZ to LZ cell ratio among the gated populations. Error bars indicate SEM of $n = 6$ mice. (C) GSEA analysis showing the enrichment of gene signatures for DZ genes in IgE+ cells and for LZ genes in IgG1+ cells. Gene sets were derived from the DEG of the LZ/DZ array. All nominal P-values and FDR rates were <0.001. (D) Kinetics of BrdU incorporation in total (top) and DZ (bottom) IgE+GFP+ and IgG1+GFP− GC cells as assessed by flow cytometry. Error bars indicate SEM of $n = 3$ mice. (E) Ratio of LZ/DZ BCR expression levels (MFI) on gated LZ (CD86hiCXCR4lo) and DZ (CD86lo-CXCR4hi) IgE+GFP+ GC cells and IgG1+GC (GFP+ and GFP−) cells. Error bars indicate SEM of $n = 6$ mice. (F) Immunohistology of frozen mLN sections from day 11 after infection with *N. brasiliensis* to show the distribution of IgE+ and IgG1+ cells (green) in the LZ (CD35+, red) and DZ of the GC. Bar, 50 µm. (G–J) Apoptosis assay performed using the CaspGLOW active Caspase Staining kit. (G) Flow cytometry analysis showing the frequency of apoptotic cells (CaspGLOW+) among the gated populations. (H) Quantification of cell apoptosis (CaspGLOW+). Error bars indicate SEM of $n = 5$ mice. (I) Apoptotic cell distribution in the CXCR4hi and CXCR4lo compartments of the gated populations. (J) Percentage of apoptotic DZ cells among total apoptotic cells (DZ plus LZ) in IgE+GFP+ and IgG1+GFP− GC cells. Error bars indicate SEM of $n = 5$ mice. Data are representative of at least five independent experiments (A, B, and E), two independent experiments (D and F), and three independent experiments (G–J). *, $P < 0.05$; **, $P < 0.01$; ***, $P < 0.001$. (K and L) DZ to LZ ratio in silico. (K) DZ to LZ ratio when selection of IgE GC cells in the LZ was reduced to 30%. (L) DZ to LZ ratio when IgE DZ cells failed to up-regulate CXCR5 and migrate to the LZ. (M) Frequency of total apoptotic IgE+ and IgG1+ GC cells (left), apoptosis in the DZ (middle), and apoptosis in the LZ (right) resulting from impaired DZ to LZ output in silico. Data represent mean and SD of 30 simulations (K–M).

second scenario where IgE+ DZ cells failed to respond to LZ-derived CXCL13 and were thus retained in the DZ, the experimentally observed DZ/LZ distribution of IgE+ cells was successfully replicated by the in silico model (Fig. 6 L). In accordance with the experimental data, the reduced DZ to LZ output of IgE+ cells in silico was associated with increased rates of apoptosis among this population and similar percentage of apoptotic IgE+ cells in LZ and DZ (Fig. 6 M). As the DZ/LZ ratio of IgE+ cells is ∼6 (Fig. 6 B), this percentage distribution is consistent with most apoptotic IgE+ cells residing in the DZ.

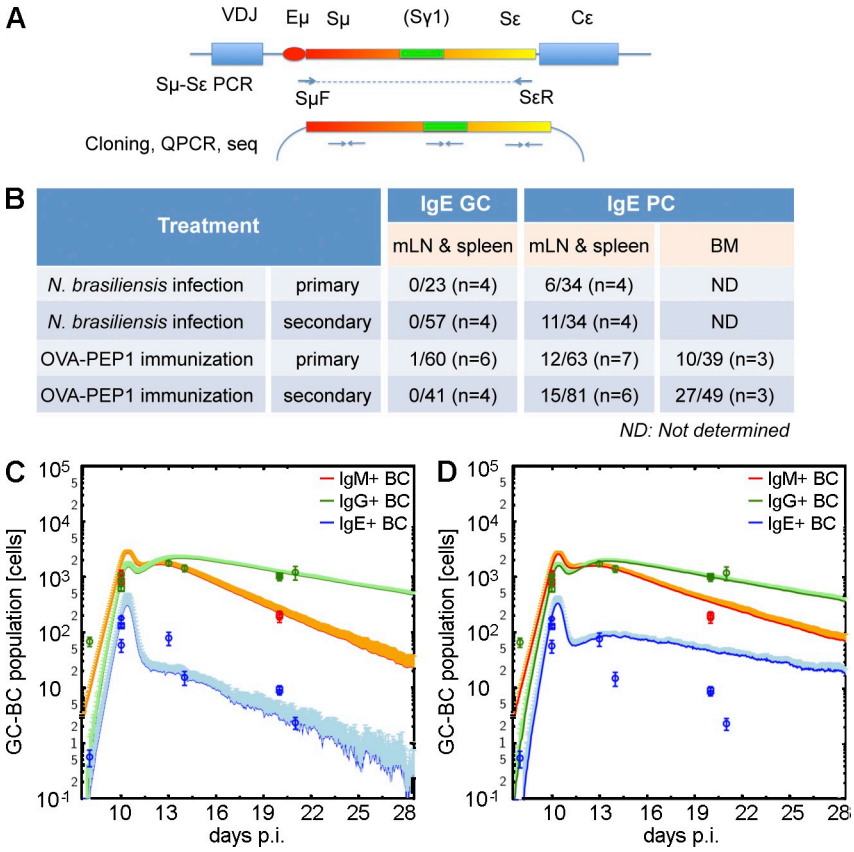

Treatment		IgE GC	IgE PC	
		mLN & spleen	mLN & spleen	BM
N. brasiliensis infection	primary	0/23 (n=4)	6/34 (n=4)	ND
N. brasiliensis infection	secondary	0/57 (n=4)	11/34 (n=4)	ND
OVA-PEP1 immunization	primary	1/60 (n=6)	12/63 (n=7)	10/39 (n=3)
OVA-PEP1 immunization	secondary	0/41 (n=4)	15/81 (n=6)	27/49 (n=3)

ND: Not determined

Figure 7. Direct switching origin of IgE⁺ GC cells: molecular and in silico analysis. (A) Schematic representation of Sγ1 footprint analysis. The switched Sμ-Sε DNA fragments were PCR amplified from purified cells that contained rearrangements to Sε (IgE⁺ and IgG1⁺GFP⁺) and the PCR products were subsequently cloned. Clones containing Sμ-Sε switch regions were identified by QPCR analysis of μ-enhancer and Sε sequences. The presence of Sγ1 sequences was determined by QPCR or DNA sequencing. (B) Sγ1 DNA repeat "footprints" in the Sμ-Sε fragment of IgE⁺ cells. Sγ1⁺ clones among Sμ-Sε DNA clones in IgE⁺ cells sorted from mice after primary and secondary infection/immunization. Mice were subjected to secondary infection at 30–32 d after primary infection or secondary immunization at day 35 after primary immunization. IgE⁺ GC cells were sorted from pooled mLN and spleen, and IgE⁺ PCs were sorted from pooled mLN and spleen or BM. n = 3–7 mice per group total pooled from two to three independent experiments. (C) Direct switching model in silico. The graph shows the population kinetics of IgE⁺ GC cells when they were originated from IgM⁺ but not IgG1⁺ GC precursor cells. (D) Sequential switching model in silico. The graph shows the population kinetics of IgE⁺ GC cells if they were originated from IgG1⁺ but not IgM⁺ GC precursor cells. Data represent mean and SD of 30 simulations (C and D).

Both the experimental and in silico analyses of IgE⁺ GC B cells reported here support a model in which reduced DZ to LZ output of IgE⁺ cells drives the distinct DZ/LZ distribution of this population. Reduced expression of the BCR and other costimulatory molecules in IgE⁺ GC cells may simultaneously contribute to the impaired selection of these cells in the LZ.

Direct versus sequential switching origin of IgE⁺ GC cells and IgE⁺ PC

We previously demonstrated that sequential switching is the main mechanism to generate high affinity IgE antibodies (Erazo et al., 2007; Xiong et al., 2012b), so we next investigated whether direct switching and sequential switching had different roles to play in the generation of IgE⁺ GC cells and IgE⁺ PC. Genetic evidence of SμSγ1→Sε sequential switching can be determined by the presence of Sγ1 DNA remnants in the Sμ-Sε region of IgE⁺ cells (Xiong et al., 2012b; Fig. 7 A). Analysis of Sμ-Sε DNA fragments in GC cells obtained during primary and secondary responses to *N. brasiliensis* infection (BALB/c mice) or immunization (TBmc mice) demonstrated an almost complete absence of Sγ1 remnants (Fig. 7 B). In contrast, Sγ1⁺ clones were consistently detected among Sμ-Sε DNA clones from IgE⁺ PC harvested during primary and secondary responses (Fig. 7 B). The highest frequency of Sγ1 remnants (~50%) was found in BM IgE⁺ PC after secondary immunization (Fig. 7 B). It should be noted here that only a fraction of SμSγ1→Sε junctions retain Sγ1 DNA (Xiong et al., 2012b); hence, the percentages indicated above underestimates the true extent of sequential switching. These results indicated that IgE⁺ GC cells are generated by direct switching of IgM⁺ cells, whereas sequential switching from IgG1⁺ cells gives rise to IgE⁺ PC, even during primary immunization.

We next investigated the implications of these data by testing different models of CSR under distinct sets of GC kinetic conditions in silico. The population dynamics required to induce a steep decline in IgE⁺ GC cells could only be achieved when the IgE⁺ GC cells originated from IgM⁺ precursors (Fig. 7 C) but not IgG1⁺ precursors (Fig. 7 D). In this model, the IgM⁺ cells switched to either IgG1 or IgE with assigned probabilities of p_{MG} = 0.04 and p_{ME} = 0.01, respectively. IgG1⁺ GC cells were assumed to sequentially switch to IgE with probability p_{GE}. In simulations with $p_{GE} > 0$, the population kinetics of IgE⁺ GC B cells matched the population kinetics of the IgG1⁺ cells, even when IgE⁺ B cells failed selection at a rate of 100%. Thus, the mathematical analyses predicted that IgE⁺ GC B cells are derived from IgM⁺ B cells, and that IgG1⁺ GC B cells do not switch to IgE before exiting the GC. Collectively, both the molecular and in silico analyses support a direct switch origin for IgE⁺ GC cells.

We then determined whether IgE⁺ and IgG1⁺ GC and PC cells displayed different rates of somatic hypermutation and affinity maturation. Analysis of the heavy chain VDJ gene

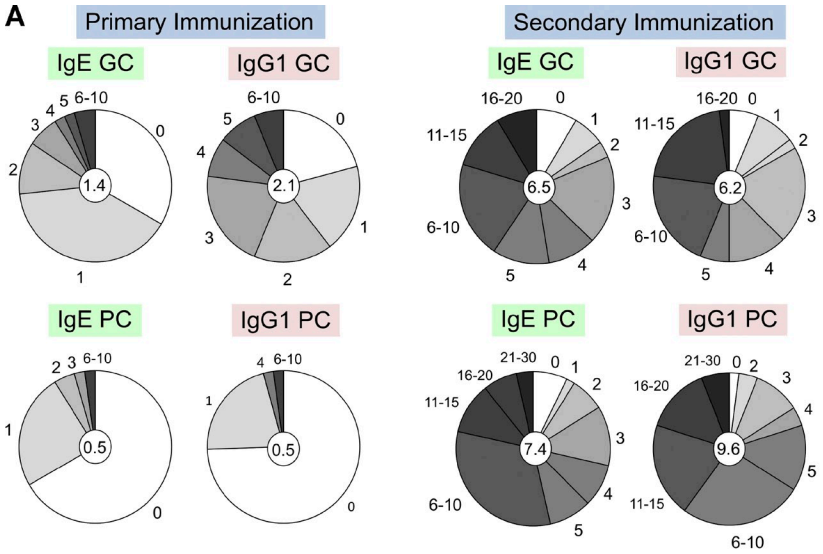

C

Ig isotypes	Residues	Primary (D12)		Secondary(D7)	
		GC	PC	GC	PC
IgE n=45-59	R97	98	100	90	96
	R97T	0	0	2	2
	R97nonT	2	0	8	2
	N100	98	98	92	96
	N100S/T	2	0	5	4
	N100nonS/T	0	2	3	0
	A101	100	96	78	93
	A101T	0	0	3	5
	A101nonT	0	4	19	2
IgG1 n=47-50	R97	92	98	90	60
	R97T	2	0	2	24
	R97nonT	6	2	8	16
	N100	98	100	100	64
	N100S/T	0	0	0	32
	N100nonS/T	2	0	0	4
	A101	98	100	81	88
	A101T	0	0	0	8
	A101nonT	2	0	19	4

Figure 8. IgE⁺ GC cells are capable of acquiring affinity enhancing maturations. (A) Analysis of VDJ nucleotide mutations in sorted IgE⁺ and IgG1⁺ cells from TBmc mice after primary (day 12) and secondary (day 7) immunization with OVA-PEP1. Mice were subjected to secondary immunization 33 d after primary immunization. The pie charts show the proportion of sequences carrying the indicated number of nucleotide mutations/sequence (n = 45–59 sequences per group). The mean number of mutations is shown in the center of each pie chart. (B) Analysis of VDJ amino acid mutations in sorted IgE⁺ and IgG1⁺ cells from TBmc mice after primary (day 12) and secondary (day 7) immunization with OVA-PEP1. The bar graph shows the mean number of amino acid mutations per sequence. Error bars represent SEM of n = 45–59 sequences per group. *, $P < 0.05$; ***, $P < 0.001$. (C) The table shows the frequency of CDR3 high affinity mutations (in red).

mutations in IgE⁺ and IgG1⁺ GC cells indicated higher frequencies of nucleotide and amino acid mutations during primary immunizations in IgG1⁺ GC cells compared with IgE⁺ GC cells (Fig. 8, A and B). IgE⁺ and IgG1⁺ GC cells carried slightly higher numbers of nucleotide and amino acid mutations per sequence than did PC after primary immunization, whereas the reverse was true for IgG1⁺ cells during secondary immunization (Fig. 8, A and B). The frequency of high affinity amino acid mutations was increased in IgG1⁺ PC compared with IgE⁺ PC (Fig. 8 C), consistent with previous observations (Erazo et al., 2007; Yang et al., 2012). Our results demonstrate that IgE⁺ GCs are not intermediates in the generation of high affinity IgE⁺ PC through sequential switching, and that IgE⁺ GC cells are not hampered in their capacity to acquire affinity enhancing mutations.

IgE⁻B220⁺ switched B cells and IgE⁺ PC are the main contributors to IgE memory

The impaired GC phase of the IgE response led us to hypothesize that conventional IgE memory cells might not exist (Erazo et al., 2007; Xiong et al., 2012a,b), a concept challenged in recent publications (Lafaille et al., 2012; Talay et al., 2012). Because markers for memory IgE⁺ cells could potentially differ from markers of other memory B cell populations (Kurosaki et al., 2010), we next established a marker-independent method for determining whether IgE⁺B220⁺CD138⁻ cells (containing both GC and putative memory cells) could contribute to a secondary antibody response. For this purpose we purified HA-specific, IgE-depleted IgM⁻IgD⁻B220⁺CD138⁻ cells and IgE-containing total IgM⁻IgD⁻B220⁺CD138⁻ cells from TBmc mice immunized 3 wk earlier (Fig. 9 A; and Fig. S2, A and B). The purified B cells were transferred to BALB/c mice together with naive OVA-specific T cells, and the mice were subsequently immunized with OVA-HA. Two weeks later, serum levels of HA-specific IgE were assayed and found to be comparable between the mouse groups that received switched B220⁺ B cells irrespective of whether the transplanted cells included IgE⁺ B cells (Fig. 9 B). The two groups of mice also exhibited similar levels of HA-specific IgE transcripts in LN, spleen, and BM (Fig. 9 C). Under these conditions, the contribution of endogenous lymphocytes to the HA-specific IgE and IgG1 responses was undetectable (Fig. 9, B and C). These results indicate that the contribution of IgE⁺B220⁺CD138⁻ cells to the IgE recall response is negligible.

We next investigated whether IgE-depleted PC from spleen and LN were capable of generating an IgE response

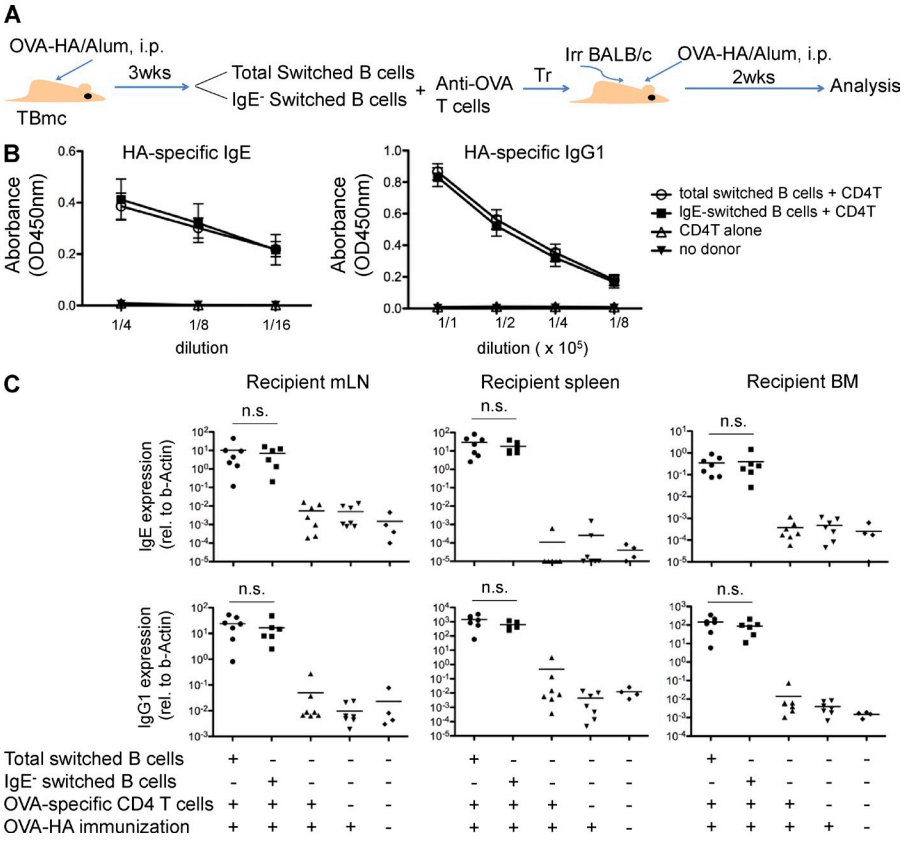

Figure 9. IgE recall responses depend primarily on de novo sequential switching rather than on memory IgE+ B cells. (A) Schematic of transfer experiments in B and C. TBmc mice were immunized with OVA-HA in alum and switched B cells were isolated from pooled spleen and mLN on day 21 after immunization. 2 × 10^6 switched B cells ($B220^+CD138^-IgM^-IgD^-$) or IgE-depleted switched B cells were injected i.v. into irradiated BALB/c mice together with 1 × 10^5 naive OVA-specific $CD4^+$ T cells. Recipient mice and the control mice that received $CD4^+$ T cells only (or no donor cells at all) were immunized with OVA-HA in alum. (B) Antigen-specific serum IgE and IgG1 antibody levels in recipient mice as assessed by ELISA 2 wk after transfer. Error bars indicate SEM. (C) QPCR measurement of mature Cε and Cγ1 transcripts in mLN, spleen, and BM of recipient mice 2 wk after cell transfer. Each symbol represents an individual mouse; horizontal lines indicate the mean. *n* = 4–7 mice per group from three independent experiments (B and C).

comparable to their $CD138^-$ counterparts. Purified IgE^- PC or IgE^+ PC cells from immunized TBmc mice were transferred into BALB/c mice that received no further treatment (Fig. 10 A; and Fig. S2, C and D). Two weeks later, the mice that had been injected with purified IgE^+ PC displayed significantly higher levels of serum HA-specific IgE antibodies and HA-specific IgE transcripts in spleen and BM than mice that had received IgE^- PC (Fig. 10, B and C). IgE antibodies were still detected in serum up to 60 d after transfer (Fig. 10 D). IgE^- PC transferred production of HA-specific IgG1 antibodies but not production of HA-specific IgE antibodies (Fig. 10 B), confirming that $IgG1^+$ PCs are terminally differentiated and unable to undergo CSR. Although donor IgE^+ PC contributed markedly less to HA-specific serum Ig than did donor $IgG1^+$ cells, these data clearly demonstrate that IgE^+ PCs mediate the long-term production of serum IgE. Our results are consistent with the concept that classical memory IgE cells are mostly absent in mice, and that IgE memory relies predominantly on de novo switching from non-IgE^+ cells and on the maintenance of long-lived IgE^+ PC.

DISCUSSION

In this study, we investigated CSR to IgE in vivo using a new reporter mouse strain that marks all cells carrying rearrangements to Sε. We described novel findings on the developmental origin, phenotype, and function of IgE^+ GC cells that explain their rapid decline and failure to contribute to the memory of IgE responses, and the specific role played by $IgG1^+$ cells in the ultimate generation of IgE^+ PC.

We observed striking differences between the population kinetics of IgE^+ and $IgG1^+$ GC B cells during a primary immune response, similar to previous findings from Yang et al. (2012). However, although these authors proposed that the rapid decline in IgE^+ GC cell frequency was likely due to their differentiation to PC, we now provide evidence for an alternative model in which IgE^+ GC cells are unfit to engage in the dynamics of the mature GC and are rapidly depleted by high rates of apoptosis. We propose that this phenotype is primarily conferred by impaired BCR expression and function in IgE^+ GC cells. In addition, we identified striking differences in the switch origin of IgE^+ GC cells and IgE^+ PC that further question the ability of IgE^+ GC cells to give rise to IgE^+ PC.

Our analysis of Sμ-Sε switch junctions revealed that IgE^+ GC cells are the product of direct class switching, with virtually no Sγ1 remnants evident in the Sμ-Sε junctions after either primary or secondary responses. The IgE^+ GC cells present after secondary immunization exhibited more extensive VDJ mutations than after primary immunization. One possibility to explain these findings is that IgM^+ memory cells (Dogan et al., 2009; Pape et al., 2011), rather than IgM naive cells, generate IgE^+ GC cells in secondary immunization. The IgM memory would respond faster than naive cells to the secondary challenge. In addition (and non–mutually exclusively) the newly generated IgE^+ GC cells may rapidly acquire

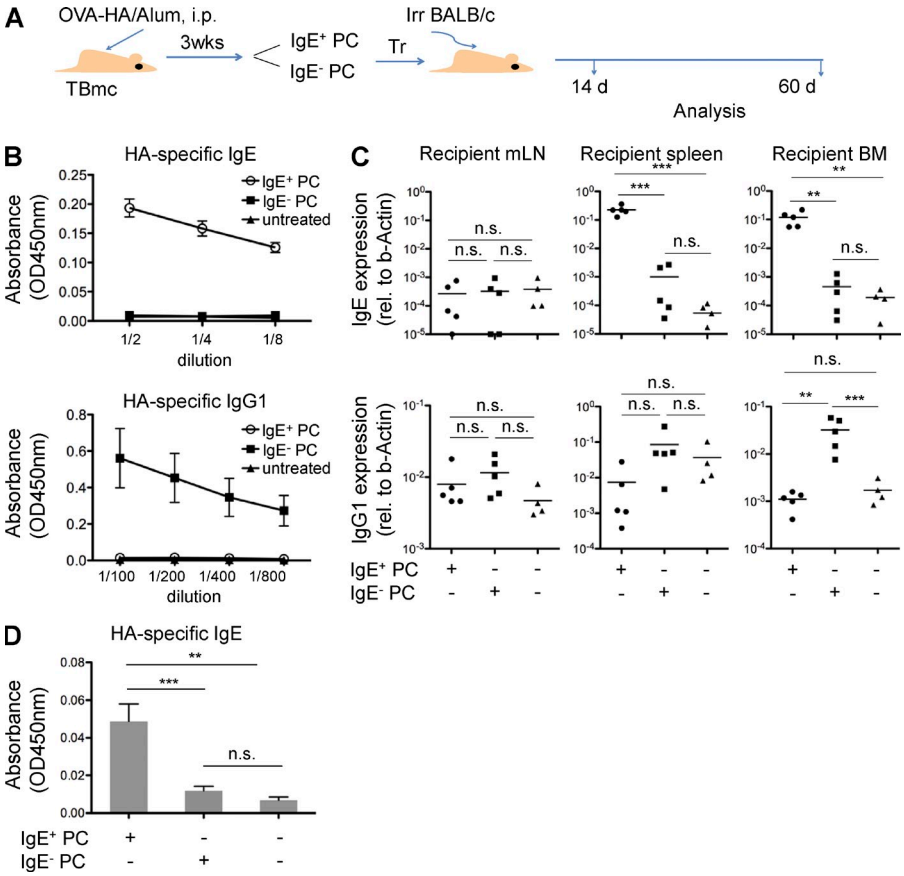

Figure 10. Evidences of BM-homing IgE+ PCs. (A) Schematic of transfer experiments in B–D. TBmc mice were immunized with OVA-HA in alum and 10^5 IgE+ PC ($B220^{lo}CD138^+$) or IgE− switched PC ($IgM^-B220^{lo}CD138^+$) were sorted from pooled spleen and mLN on day 21 after immunization and injected i.v. into irradiated recipient BALB/c mice. (B) HA-specific IgE and IgG1 serum antibody levels in recipient mice 2 wk after cell transfer as determined by ELISA. Error bars indicate SEM. (C) QPCR measurement of mature Cε and Cγ1 transcripts in mLN, spleen, and BM from recipient mice at 2 wk after transfer. Each symbol represents an individual mouse; horizontal lines indicate the mean value. (D) Serum HA-specific IgE levels at 60 d after transfer as determined by ELISA. Serum samples were subjected to twofold predilution. Error bars indicate SEM. Data are representative of two independent experiments (n = 4–5 mice per group per experiment; B–D). **, P < 0.01; ***, P < 0.001.

mutations due to enhanced T cell help and the presence of preexisting GC structures. Alternatively, it is also possible that a few IgE+ GC cells survive after the primary immunization and can transiently expand during a recall response.

In contrast to IgE+ GC cells, Sγ1 remnants were identified in 20–30% of the Sμ-Sε junctions in IgE+ PC in spleen and LN, and in up to 50% of IgE+ PC in BM, indicating a sequential switching origin for these populations. Because Sγ1 sequences may be lost during SμSγ1-Sε switching, the frequency of sequential switching is always partially underestimated by the quantification of Sγ1 remnants. Sequentially switched PC cells can never be generated by directly switched GC cells because the entire Sγ1 DNA is deleted upon direct Sμ-Sε switching. A substantial fraction of the IgE-producing PC cells must therefore have distinct origins from those of IgE+ GC cells. Based on the population kinetics of these subsets, similar conclusions on the precursor origins of IgE+ GC cells and IgE+ PC were also reached via our mathematical modeling approaches.

We report here that IgE+ GC cells express three- to fourfold lower levels of BCR than do IgG1+ GC cells, as well as exhibiting a comparatively reduced BCR signaling response to H_2O_2. We propose that these deficiencies contribute to the high levels of apoptosis observed among IgE+ GC cells. BCR-mediated antigen uptake is essential for antigen presentation to Tfh cells and subsequent clonal selection in the GC (Victora and Nussenzweig, 2012). BCR signaling is also believed to be necessary during the GC reaction, although it is not yet clear how and when this occurs. Both processes (BCR-mediated antigen uptake and BCR signaling) share a requirement for signaling molecules such as Syk (Hou et al., 2006; Vascotto et al., 2007). It has been suggested that BCR signaling-dependent checkpoints take place in the G2/M phase during each replication cycle (Khalil et al., 2012). Because GC cells in G2/M are in the DZ (Victora et al., 2010), BCR signaling would occur in the DZ. Thus, impaired signaling in IgE+ DZ cells may drive the higher incidence of apoptosis that we observed among these cells.

DZ cells may also require BCR function (antigen capture, signaling, or antigen presentation) to successfully up-regulate CXCR5 and transition into the LZ. We observed that strikingly few IgE+ cells in the GC exhibited a characteristic LZ phenotype. The DZ and LZ composition of GCs is determined by rates of B cell proliferation, selection, differentiation, and interzonal migration (Meyer-Hermann et al., 2006, 2012; Figge et al., 2008; Garin et al., 2010; Victora et al., 2010; Zhang et al., 2013). LZ cells are selected to differentiate into memory or PCs, or to recycle to the DZ, whereas nonselected cells undergo apoptosis. In the DZ these cells instead mutate and undergo rapid clonal expansion. A higher proportion of DZ than LZ cells engages in intra-zonal migration, producing a net migration of cells from DZ to the LZ (Victora et al., 2010).

Using mathematical analyses, we tested whether the low frequency of IgE$^+$ LZ cells could be accounted for by impaired LZ selection into the recycling pool, or by decreased DZ to LZ migration. We found that the best-fit model for the observed DZ/LZ distribution of IgE$^+$ GC cells was generated by a decreased DZ to LZ output. It has previously been reported that low-affinity GC B cells are retained in the LZ during competition with high affinity B cells (Victora et al., 2010). The phenotype of IgE$^+$ GC cells therefore appears to result from an intrinsic defect in fitness/survival rather than a lack of affinity maturation, or differentiation into PC.

The high apoptosis of IgE$^+$ GC cells may partially explain the dominance of the PC component in IgE responses. However, as previously suggested, an increased tendency of IgE$^+$ cells to differentiate into PC may also play a role, and we have shown that sequential switching from IgG1$^+$ cells is coupled to IgE$^+$ PC differentiation. IgE$^+$ PC comprise ∼20–40% of the total PC population in spleen and LN, similar to IgG1$^+$ PC. Because class switching to IgE occurs with much lower probability than class switching to IgG1 (Siebenkotten et al., 1992; Hackney et al., 2009), the high frequency of IgE$^+$ PC suggests a higher rate of differentiation to PC than IgG1$^+$ cells.

The observation in a recent report that the steep decline in IgE$^+$ GC cells was not prevented that by Bcl2 transgene overexpression was considered as proof that IgE$^+$ GC cell numbers decrease due to differentiation into PC (Yang et al., 2012). However, earlier investigations in Bcl2 transgenic mice reported that despite exhibiting normal GC size, these animals also display restricted proliferation of GC cells in addition to impaired GC apoptosis (Smith et al., 1994, 2000). Furthermore, Bcl2 overexpression led to an increase in the number of memory B cells and PC cells with low antigen affinity (Smith et al., 1994, 2000). It was concluded that the Bcl2 overexpression rescued low affinity GC cells into the memory and PC compartments. These complex effects of Bcl2 overexpression thus make it difficult to interpret its role in IgE$^+$ GC cells. In the current report, we demonstrate that IgE$^+$ GC cells undergo affinity maturation, but their numbers are decreased in the LZ where Tfh-mediated selection into memory cells and high affinity PC occurs. Thus, IgE$^+$ GC cells in the LZ may not reach the differentiation stage at which they might benefit from transgenic Bcl2 expression.

To determine whether IgE$^+$ GC cells contribute to the memory pool and long-lived PC compartments, we performed adoptive transfer experiments using B220$^+$ switched B cells either containing or lacking IgE$^+$ cells. We determined that IgE$^+$B220$^+$ cells did not significantly contribute to secondary IgE antibody responses in transplanted animals. Rather, IgE antibodies were generated by the sequential switching of IgG1$^+$ cells. It was previously reported that the production of IgE, but not IgG1, during secondary immune responses requires IL-4, suggesting that de novo switching to IgE is necessary for recall responses (Finkelman et al., 1988). Contrasting with these results, Talay et al. (2012) used an IgE-IRES-GFP reporter mouse to determine that IgE$^+$ memory cells, and not other B cells, mediated secondary IgE responses. However, the model used by these authors included the addition of a human membrane exon and the replacement of key polyadenylation sites in the IgE locus that may have modified antibody expression and/or altered the biology of IgE-producing cells in these animals (Lafaille et al., 2012).

The existence of long-lived IgE$^+$ PC has been controversial (Achatz-Straussberger et al., 2008; Luger et al., 2009; Yang et al., 2012), and our current findings now demonstrate that IgE$^+$ PC contribute to long-term production of serum IgE, albeit less efficiently than do IgG1$^+$ PC. This may be due to increased apoptosis or inefficient BM homing of IgE$^+$ PC (Achatz-Straussberger et al., 2008), the lower half-life of serum IgE (Vieira and Rajewsky, 1988), and cytophilic removal of serum IgE through binding to FceRI and FceRII/CD23 (Gould and Sutton, 2008).

On average, IgE$^+$ PC exhibited fewer high affinity amino acid replacements than did IgG1$^+$ PC, which was in agreement with a delayed affinity maturation of the IgE response compared with the IgG1 response (Erazo et al., 2007; Yang et al., 2012). If most IgE$^+$ PC cells are generated from IgG1$^+$ cells, it may be that the IgG1$^+$ cells that become IgG1$^+$ PC are different (of higher affinity or different differentiation stage) than the IgG1$^+$ cells that become IgE$^+$ PC.

In sum, the data presented here on IgE GC cell phenotype and function, and on the distinct roles of direct and sequential switching in IgE$^+$GC and IgE$^+$PC differentiation, can be integrated with previous findings to construct a model of T cell–dependent IgE responses. In the initial phase of a response, direct Sμ-Sε switching from IgM$^+$ cells generates a transient wave of IgE$^+$ GC cells. A population of IgE$^+$ PC is also generated at least in part through sequential switching of IgG1$^+$ cells. As total antigen levels decrease and antigen becomes restricted to FDC depots, the generation of IgE$^+$ GC cells is halted. Reduced BCR function renders IgE$^+$ GC cells unfit to engage in the GC dynamics, resulting in higher rates of apoptosis and a rapid decline of the entire IgE$^+$ GC population. Consequently, IgE$^+$ GC cells are unable to contribute to the memory and high affinity PC compartments. In contrast, IgG1$^+$ cells can successfully engage in continuous cycles of proliferation/mutation and selection in the GC. Interactions of IgG1$^+$ GC cells or IgG1$^+$ memory cells with IL-4–producing T helper cells lead to sequential switching to IgE and rapid formation of IgE$^+$ PC. This model offers an explanation as to why the high affinity IgE response depends on sequential switching from IgG1$^+$ B cells despite the earlier generation of IgE$^+$ GC cells. It is tempting to speculate that these features of the IgE response may result from evolutionary pressure to restrict the development of IgE memory cells and yet maintain the capacity to produce limited amounts of high-affinity IgE antibodies.

MATERIALS AND METHODS

Mice. CεGFP mice were generated by gene targeting in mouse embryonic stem (ES) cells. The DNA targeting vector contained an *IRES-GFP* cassette inserted into the 3′ UTR region of the Cε gene, downstream of the M2 membrane exon and upstream of the polyadenylation sequences (Fig. S1 A). The targeting construct also contained a *neo^r-loxP* cassette inserted

in the intron between the *CH4* and *M1* exons, and an *HSV-TK* (Herpes Simplex Virus thymidine kinase) cassette at the 5′ end of the construct. The linearized vector was transfected into a clone of the 129-derived J1 ES cell line. The ES cells were then selected in medium containing G418 and ganyclovir for positive and negative selection, respectively. Colonies carrying homologous integrations were first identified by PCR using primers 5′-GACACCCCAAGAGAAGGACA-3′ (INT5F3) and 5′-GCCTGAAGAACGAGATCAGC-3′ (INT5R3), and 5′-CCCACCATCAACAGGGCTA-3′ (UpM-R), and integration was confirmed by Southern blotting. Retention of the *IRES-GFP* cassette downstream of the membrane exons was confirmed by PCR using the primers 5′-CTTGTGTAGCGCCAAGTGC-3′ (INT5R) and 5′-TTGCATTCCTTTGGCGAG-3′ (IRESR2). The *neo^r-loxP* cassette was then removed by Cre-mediated recombination before injection of the ES cells into blastocysts. Deletion of the *neo^r-loxP* cassette was confirmed by PCR using primers 5′-GTATATGTGTTCCCACCACCAGA-3′ (INT5F4) and 5′-CTGTGGTTTCCAAATGTGTCAG-3′ (INT5R4), and by the loss of resistance to G418. Mice carrying the *IRES-GFP* KI in the Cε gene, before now referred as CεGFP, were backcrossed to BALB/c mice and TBmc mice (Curotto de Lafaille et al., 2001). All the mice used in the current study were CεGFP heterozygous.

BALB/c mice were purchased from The Jackson Laboratory. Mice were bred and housed in the specific pathogen-free animal facility of the Biological Research Center (BRC) A*STAR, Singapore. All animal procedures were approved by the BRC/A*STAR Institutional Animal Care and Use Committee. 6–8-wk-old mice were used in all experiments.

Isolation of mouse naive B cells and in vitro induction of IgE production. Naive B cells were isolated from the spleens and mLN of untreated CεGFP mice, using anti-CD43 MicroBeads (Miltenyi Biotec) and magnetic cell sorting. A total of 0.25×10^6/ml of purified cells were stimulated with 20 μg/ml LPS (Sigma Aldrich) and 10 ng/ml IL-4 (R&D Systems) or with 3 μg/ml anti-CD40 antibodies (eBioscience) and 5 ng/ml IL-4 for 4–5 d in vitro.

Immunizations and infections. CεGFP TBmc mice and TBmc mice were immunized by i.p. injection of 100 μg OVA-HA (chicken ovalbumin cross-linked to HA peptide YPYDVPDYASLRS) or 100 μg OVA-PEP1 (chicken ovalbumin cross-linked to the low affinity PEP1 peptide YPYDVPDFASLRS) in alum (Erazo et al., 2007). CεGFP BALB/c and WT BALB/c mice were infected with 500 L3 larvae of *N. brasiliensis* via subcutaneous route as previously described (Camberis et al., 2003).

Microarray analysis. NA was isolated from sorted B cell subsets using Arcturus Picopure (Life Technologies) RNA Purification kits. RNA quality was assessed by Bioanalyzer (Agilent Technologies). SPIA cDNA were prepared from 2 ng of total RNA using the Ovation Pico WTA system (v2; NuGEN) kit protocol before fragmentation and labeling according to the Encore Biotin kit (NuGEN) protocol.

Sample hybridization was performed on MoGene 1.0 ST arrays (Affymetrix; accession no. GSE49033). Data were normalized with RMA and differential gene analysis was performed using limma. Both of these analyses and the χ^2 test for set overlap significance were performed in R (v2.15.2; Smyth, 2004). Expression heat-maps were generated with the Multi Experiment Viewer (Saeed et al., 2003). GSEA was performed with the GSEA software from the BROAD institute using default parameters and gene set-based permutation tests (Mootha et al., 2003; Subramanian et al., 2005). All data handling and analysis was facilitated by Pipeline Pilot (Accelrys).

Flow cytometry analysis and cell sorting. Staining of IgE$^+$ cells was preceded by a brief acid treatment to remove FcεRII/CD23-bound IgE as described previously (Erazo et al., 2007). Staining with the anti-IgE antibody R1E4 (Keegan et al., 1991) did not require acid treatment because R1E4 does not recognize IgE bound to CD23 or FcεRI (Mandler et al., 1993). All staining of IgE$^+$ cells for use in functional analyses (signaling and apoptosis assays or adoptive transfer experiments) was performed using the anti-IgE antibody R1E4.

Single cell suspensions were incubated with 10 μg/ml anti-CD16/32 for 15 min at 4°C before surface labeling with antibody cocktails in staining buffer (2% FBS, 4 mM EDTA, and 0.1% NaN_3) for 30 min at 4°C. Intracellular staining was conducted using Cytofix/Cytoperm kits (BD). Cells were analyzed using LSR II 4/5-laser flow cytometer (BD) or sorted using a FACSAria II 4/5-laser cell sorter (BD). Purified cells were used for signaling assays ex vivo, for expression analysis using microarrays or QPCR, or for adoptive transfer into recipient mice.

BrdU proliferation assay. Mice were infected with *N. brasiliensis* for 10 d and subjected to i.p. injection with 3 mg BrdU. After 4-8 h, the mLN were collected and BrdU incorporation was analyzed using BrdU Flow kits (BD).

Apoptosis assays. 10^6 freshly isolated mLN cells from infected or immunized mice were resuspended in 1 ml RPMI-based complete medium, and then immediately mixed with Red-VAD-FMK (CaspGlow; BioVision) and incubated for 45 min at 37°C in 5% CO_2. Cells were then stained with antibodies against B220, CD138, IgE, and IgG1, and then analyzed in a 5-laser LSR II apparatus. For the active Caspase3 assay, freshly isolated mLN cells from infected or immunized mice were surface-labeled with antibodies against B220, CD138, IgE, and IgG1 and then fixed, permeabilized, and stained for intracellular active Caspase3 and GFP. Cells were analyzed by flow cytometry using a LSR II apparatus.

Quantification of B cell receptor levels in IgE and IgG1 cell. Single-cell suspensions were prepared from the mLN of OVA-HA–immunized CεGFP TBmc mice and then incubated with Alexa Fluor 647–anti-IgE (R1E4), PerCP-eFluro710–anti-IgG1, PE–anti-CD138, APC-eFluro780–anti-B220, eFluro650–anti-IgM, eFluro450–anti-IgD, and biotin-labeled HA peptide (0–1,000 ng/ml) at 4°C for 30 min, followed by addition of streptavidin-PE.Cy7. The samples were then analyzed using a LSR II apparatus.

Ex vivo stimulation and analysis of phospho-signaling proteins. Single cell suspensions of mLN from infected or immunized mice were rested at 37°C in a CO_2 incubator for 30 min after isolation. The cells were then stimulated for 10 min in RPMI-based complete medium in the absence or presence of 2.5–10 mM H_2O_2 for 10 min or with 10 μg/ml OVA-HA for 5 min. After stimulation, the cells were immediately fixed by adding a 1:1 volume of warm Phosflow fix buffer I (BD), followed by incubation at 37°C for 10 min. Fixed cells were permeabilized by 30 min methanol treatment on ice, and then washed twice with 2% FBS-DPBS and stained with phospho-specific antibodies PE–anti-phospho-Erk1/2 (Thr202/Tyr204), PE–anti–phospho-Syk (Tyr525/526), or Alexa Fluor 647–anti-BLNK (pY84) at room temperature for 1 h. The cells were then analyzed by flow cytometry.

Immunohistology. Oct frozen mLNs were processed as described previously (Erazo et al., 2007). Sections were stained with antibodies against IgE (R1E4), IgG1 (RMG1-1), CD35 (8C12), and nuclei were counterstained with Hoechst 33342. Images were acquired with an IX81 microscope (Olympus) and Image Pro MDA software (v6.2; Media Cybernetics) at 400× magnification.

Analysis of Sg1 remnants in Sμ-Sε junctions. Genomic DNA was extracted from sorted IgE$^+$ cells and the Sμ-Sε junctions were amplified by PCR using high fidelity ExTaq Polymerase (Takara Bio Inc.) with the primers SμF and SεR (Xiong et al., 2012b). Amplified Sμ-Sε fragments were cloned into TA vector (Invitrogen), and colonies containing bona fide Sμ-Sε regions were identified by QPCR using primers specific for the μ-Enhancer region (MuEnF, 5′-AGCTTGAGTAGTTCTAGTTTCCCC-3′ and MuEnR, 5′-TGGGGACCAATAATCAGAGGG-3′) and the Sε switch region (SεF, 5′-GGGCTGCACTAAATGGGACT-3′ and SεR, 5′-GCCCGATTGGCTCTACCTAC-3′). The presence of switch Sγ1 region footprints was determined by QPCR analysis of Sγ1 repeats using Sγ1F and Sγ1R primers(Xiong et al., 2012b), or by DNA sequencing.

VDJ sequence analysis. Total RNA extraction and cDNA synthesis were performed using standard procedures with sorted cells isolated from OVA-PEP1–immunized TBmc mice. PCR analysis of cDNA was performed using ExTaq Polymerase (Takara Bio Inc.) with the forward primer 5′UTR and reverse primers specific for IgE and IgG1 constant regions, as previously described (Erazo et al., 2007).

Adoptive transfer experiments. Switched B cells were isolated from pooled spleen and mLN of TBmc mice three weeks after immunization with OVA-HA in alum. Cells were preenriched by incubating with negative selection cocktail including CD3e-biotin, CD11c-biotin, CD11b-biotin, Gr-1-biotin, and TER-119-biotin, followed by addition of streptavidin MicroBeads and magnetic depletion using the Miltenyi Biotec system. Unbound cells were then stained with Alexa Fluor 647 anti-IgE (R1E4), PerCP-eFluro710 anti-IgG1, PE anti-CD138, APC-eFluro780 anti-B220, PE.Cy7 anti-IgM, and eFluro450 anti-IgD. Total switched GC/memory cells were sorted as $IgM^-IgD^-CD138^-B220^+$ cells. IgE-switched GC/memory cells were sorted as $IgE^-IgM^-IgD^-CD138^-B220^+$ cells. At 3 wk after immunization, IgE comprised ∼1% of the $B220^+$ switched GC/memory pool. Naive OVA-specific $CD4^+$ T from untreated TBmc mice were first enriched by negative selection using a $CD4^+$ T cell isolation kit (Miltenyi Biotec) and then stained with antibodies against B220 and CD4 for further purification using an Aria II cell sorter. Sorted B cells ($\sim 2 \times 10^6$) together with 10^5 naive OVA-specific CD4 T cells were injected i.v. into γ-irradiated BALB/c mice (150 rad low dose exposure). The recipient mice, as well control mice that were either untransplanted or received T cells only, were subsequently immunized with 100 µg OVA-HA in alum. IgE-depleted $CD138^+$ plasmablasts/pre-PCs and IgE^+ $CD138^+$ cells were also sorted from immunized TBmc mice and injected i.v. into γ-irradiated naive BALB/c mice (150 rad exposure). PC recipient mice were not immunized. Spleen, mLN, BM, and serum were collected on day 14 after transfer. To investigate the existence of long-lived IgE PCs, serum was collected on day 60 after transfer. Levels of HA-specific IgE and IgG1 transcripts were analyzed by QPCR using cDNA obtained from tissue samples. Primers used for IgE transcript analysis were 17/9DJF1, 5′-GTACGACGAGAACGGGTTTG-3′ and IgE2, and the primers for IgG1 transcript analysis were 17/9DJF1 and 5′-GGATCCAGAGTTCCA-GGTCACT-3′ (Erazo et al., 2007). Serum levels of HA-specific antibodies were determined by ELISA.

RNA purification, cDNA synthesis and quantitative PCR analysis (QPCR). Tissue RNA was extracted using RNeasy mini kits (QIAGEN). cDNA was synthesized with SuperScript II reverse transcription (Invitrogen) using standard protocols. QPCR analysis was performed as previously described to assess the expression of the Cε switched transcript and Cε and Cγ1 mature transcripts for the 17/9 VDJ KI genes of TBmc mice (Erazo et al., 2007). The following primers were used for quantification of secreted and membrane Ig: secreted IgE, 5′-GTCGCCTAGAGGTCGCCAAG-3′ and 5′-CATCCACCTTCCCCACCACAGC-3′; membrane IgE, 5′-CGCC-TAGAGGTCGCCAAGAC-3′ and 5′-AGCTCACACTGAGCAGGAAC-3′; secreted IgG1, 5′-TGCACAACCACCATACTGAGA-3′ and 5′-GGG-TGGAGGTAGGTGTCAGA-3′; membrane IgG1, 5′-TGCACAACCAC-CATACTGAGA-3′ and 5′-CCTCAGCACAGGTCTCGTC-3′. The VDJ primers 5′-TGAAACTCTCCTGTGCAGCCTC-3′ and 5′-TGCAGAG-ACAGTGACCAGAGT-3′ were used to quantify total mature IgH transcripts in purified IgE^+ and $IgG1^+$ cells from TBmc mice. Expression values in each sample were normalized to β-actin.

Antigen-specific IgE and IgG1 ELISA. HA-specific IgE and IgG1 antibodies were quantified by ELISA as previously described (Curotto de Lafaille et al., 2001). To measure HA-specific IgE, serum samples were first depleted of IgG antibodies by incubation with GammaBind Plus Sepharose (GE Healthcare).

Mathematical model of GC B cell class switch and implications. An agent-based model was developed in which every B cell displayed individual dynamics of interaction and development in 3D space and time, with a particular emphasis on B cell class switching. The parameters of B and T cell migration were set based on data from intravital multi-photon imaging experiments (Figge et al., 2008). B cell selection in the LZ relies on affinity-dependent collection of antigen from follicular DCs and subsequent processing and presentation to TFH; hence, affinity-dependent competition for TC help is an integral component of the selection process (Meyer-Hermann et al., 2006; Victora et al., 2010). Zoning of the GC is derived from distinct patterns of chemokine distribution (Allen et al., 2004; Meyer-Hermann et al., 2012). B cell division and fate decision relies on asymmetric distribution of previously collected antigen between the daughter cells (Meyer-Hermann et al., 2012; Thaunat et al., 2012). All parameters used in these simulations have been described in detail elsewhere (Meyer-Hermann et al., 2012).

The model developed in the current report added a more complex motility concept to apoptotic B cells. The phagocytosis rate of apoptotic cells was determined by the overall frequency of apoptotic B cells in the experiments. The migration model of apoptotic LZ B cells (of any Ig-class) was configured to match the experimentally observed DZ/LZ ratio of apoptotic $IgG1^+$ cells.

The switch model used in the current report includes the addition of a property of the C++ B cell class. After every division event, class switch occurs with a probability given by a transformation matrix (the precise parameters are discussed in the main text). Because IgE^+ GC cells were found to express threefold less BCR molecules than $IgG1^+$ cells, the probability of binding antigen was correspondingly reduced for the IgE^+ population. Nonlinear changes of the binding probability were also tested. The lack of BCR signaling observed in vivo was implemented in silico by defining the failure of IgE^+ DZ B cells to become sensitized to CXCL13 upon differentiation to the LZ phenotype. This assumption was capable of replicating the DZ/LZ ratio of IgE^+ GC cells observed in the experimental data. Each set of simulation conditions was tested 30 times with different random number seeds and then evaluated by calculation of mean and standard deviation.

Statistics. Statistical significance was determined using Student's *t* tests (unpaired, two-tailed) in Prism 5 (GraphPad Software).

Online supplemental material. Fig. S1 describes the CεGFP KI construct and the validation of GFP expression during in vitro induction of CSR to IgE. Fig. S2 shows sorting gates and Ig transcript analysis in sorted donor IgE^+ and IgE^- cells. A list of antibodies used is provided in Table S1. DZ and LZ gene signatures derived from $IgG1^+$ GC cells (related to Fig. 6) are provided in Table S2. Online supplemental material is available at http://www.jem.org/cgi/content/full/jem.20131539/DC1.

We thank Gabriel Victora, Sidonia Fagarasan, Daniel Mucida, Tomohiro Kurosaki, Gennaro de Libero, and members of our laboratory for comments on the manuscript. We thank Anis Larbis and the flow facility, and Francesca Zolezzi and the Functional Genomics groups at SIgN for their essential support, Neil McCarthy of Insight Editing London for English editing assistance, and Graham Le Gros and Helen Mearns for the R1E4 hybridoma.

H. Xiong received a B. Levine scholarship. M. Meyer-Hermann was supported by the Bundesministeriums für Bildung und Forschung GerontoSys initiative and by the Human Frontier Science Program. Work in the M.A. Curotto de Lafaille laboratory is funded by SIgN-A*STAR core fund.

The authors have no competing financial interests.

Submitted: 20 July 2013
Accepted: 23 October 2013

REFERENCES

Achatz-Straussberger, G., N. Zaborsky, S. Königsberger, E.O. Luger, M. Lamers, R. Crameri, and G. Achatz. 2008. Migration of antibody secreting cells towards CXCL12 depends on the isotype that forms the BCR. *Eur. J. Immunol.* 38:3167–3177. http://dx.doi.org/10.1002/eji.200838456

Allen, C.D., K.M. Ansel, C. Low, R. Lesley, H. Tamamura, N. Fujii, and J.G. Cyster. 2004. Germinal center dark and light zone organization is mediated by CXCR4 and CXCR5. *Nat. Immunol.* 5:943–952. http://dx.doi.org/10.1038/ni1100

Baskin, B., K.B. Islam, B. Evengård, L. Emtestam, and C.I. Smith. 1997. Direct and sequential switching from mu to epsilon in patients with Schistosoma mansoni infection and atopic dermatitis. *Eur. J. Immunol.* 27:130–135. http://dx.doi.org/10.1002/eji.1830270120

Camberis, M., G. Le Gros, and J. Urban Jr. 2003. Animal model of *Nippostrongylus brasiliensis* and *Heligmosomoides polygyrus*. *Curr. Protoc. Immunol.* Chapter 19:12.

Curotto de Lafaille, M.A., and J.J. Lafaille. 2010. The biology of IgE: The generation of High Affinity IgE Antibodies. In Cancer and IgE: Introducing the Concept of AllergoOncology. M.L. Penichet, and E. Jensen-Jarolim, editors. Springer. 37–46.

Curotto de Lafaille, M.A., S. Muriglan, M.J. Sunshine, Y. Lei, N. Kutchukhidze, G.C. Furtado, A.K. Wensky, D. Olivares-Villagómez, and J.J. Lafaille. 2001. Hyper immunoglobulin E response in mice with monoclonal populations of B and T lymphocytes. *J. Exp. Med.* 194:1349–1359. http://dx.doi.org/10.1084/jem.194.9.1349

Cyster, J.G., and C.C. Goodnow. 1995. Protein tyrosine phosphatase 1C negatively regulates antigen receptor signaling in B lymphocytes and determines thresholds for negative selection. *Immunity*. 2:13–24. http://dx.doi.org/10.1016/1074-7613(95)90075-6

Dogan, I., B. Bertocci, V. Vilmont, F. Delbos, J. Mégret, S. Storck, C.A. Reynaud, and J.C. Weill. 2009. Multiple layers of B cell memory with different effector functions. *Nat. Immunol.* 10:1292–1299. http://dx.doi.org/10.1038/ni.1814

Erazo, A., N. Kutchukhidze, M. Leung, A.P. Christ, J.F. Urban Jr., M.A. Curotto de Lafaille, and J.J. Lafaille. 2007. Unique maturation program of the IgE response in vivo. *Immunity*. 26:191–203. http://dx.doi.org/10.1016/j.immuni.2006.12.006

Figge, M.T., A. Garin, M. Gunzer, M. Kosco-Vilbois, K.M. Toellner, and M. Meyer-Hermann. 2008. Deriving a germinal center lymphocyte migration model from two-photon data. *J. Exp. Med.* 205:3019–3029. http://dx.doi.org/10.1084/jem.20081160

Finkelman, F.D., I.M. Katona, J.F. Urban Jr., J. Holmes, J. Ohara, A.S. Tung, J.V. Sample, and W.E. Paul. 1988. IL-4 is required to generate and sustain in vivo IgE responses. *J. Immunol.* 141:2335–2341.

Galli, S.J., and M. Tsai. 2012. IgE and mast cells in allergic disease. *Nat. Med.* 18:693–704. http://dx.doi.org/10.1038/nm.2755

Garin, A., M. Meyer-Hermann, M. Contie, M.T. Figge, V. Buatois, M. Gunzer, K.M. Toellner, G. Elson, and M.H. Kosco-Vilbois. 2010. Toll-like receptor 4 signaling by follicular dendritic cells is pivotal for germinal center onset and affinity maturation. *Immunity*. 33:84–95. http://dx.doi.org/10.1016/j.immuni.2010.07.005

Gould, H.J., and B.J. Sutton. 2008. IgE in allergy and asthma today. *Nat. Rev. Immunol.* 8:205–217. http://dx.doi.org/10.1038/nri2273

Hackney, J.A., S. Misaghi, K. Senger, C. Garris, Y. Sun, M.N. Lorenzo, and A.A. Zarrin. 2009. DNA targets of AID evolutionary link between antibody somatic hypermutation and class switch recombination. *Adv. Immunol.* 101:163–189. http://dx.doi.org/10.1016/S0065-2776(08)01005-5

Heng, T.S., and M.W. Painter; Immunological Genome Project Consortium. 2008. The Immunological Genome Project: networks of gene expression in immune cells. *Nat. Immunol.* 9:1091–1094. http://dx.doi.org/10.1038/ni1008-1091

Hou, P., E. Araujo, T. Zhao, M. Zhang, D. Massenburg, M. Veselits, C. Doyle, A.R. Dinner, and M.R. Clark. 2006. B cell antigen receptor signaling and internalization are mutually exclusive events. *PLoS Biol.* 4:e200. http://dx.doi.org/10.1371/journal.pbio.0040200

Jabara, H.H., R. Loh, N. Ramesh, D. Vercelli, and R.S. Geha. 1993. Sequential switching from mu to epsilon via gamma 4 in human B cells stimulated with IL-4 and hydrocortisone. *J. Immunol.* 151:4528–4533.

Karnowski, A., G. Achatz-Straussberger, C. Klockenbusch, G. Achatz, and M.C. Lamers. 2006. Inefficient processing of mRNA for the membrane form of IgE is a genetic mechanism to limit recruitment of IgE-secreting cells. *Eur. J. Immunol.* 36:1917–1925. http://dx.doi.org/10.1002/eji.200535495

Katona, I.M., J.F. Urban Jr., and F.D. Finkelman. 1988. The role of L3T4+ and Lyt-2+ T cells in the IgE response and immunity to Nippostrongylus brasiliensis. *J. Immunol.* 140:3206–3211.

Keegan, A.D., C. Fratazzi, B. Shopes, B. Baird, and D.H. Conrad. 1991. Characterization of new rat anti-mouse IgE monoclonals and their use along with chimeric IgE to further define the site that interacts with Fc epsilon RII and Fc epsilon RI. *Mol. Immunol.* 28:1149–1154. http://dx.doi.org/10.1016/0161-5890(91)90030-N

Kelsoe, G. 1996. The germinal center: a crucible for lymphocyte selection. *Semin. Immunol.* 8:179–184. http://dx.doi.org/10.1006/smim.1996.0022

Khalil, A.M., J.C. Cambier, and M.J. Shlomchik. 2012. B cell receptor signal transduction in the GC is short-circuited by high phosphatase activity. *Science*. 336:1178–1181. http://dx.doi.org/10.1126/science.1213368

Kinet, J.P. 1999. The high-affinity IgE receptor (Fc epsilon RI): from physiology to pathology. *Annu. Rev. Immunol.* 17:931–972. http://dx.doi.org/10.1146/annurev.immunol.17.1.931

Kraus, M., M.B. Alimzhanov, N. Rajewsky, and K. Rajewsky. 2004. Survival of resting mature B lymphocytes depends on BCR signaling via the Igalpha/beta heterodimer. *Cell*. 117:787–800. http://dx.doi.org/10.1016/j.cell.2004.05.014

Kurosaki, T., Y. Aiba, K. Kometani, S. Moriyama, and Y. Takahashi. 2010. Unique properties of memory B cells of different isotypes. *Immunol. Rev.* 237:104–116. http://dx.doi.org/10.1111/j.1600-065X.2010.00939.x

Lafaille, J.J., H. Xiong, and M.A. Curotto de Lafaille. 2012. On the differentiation of mouse IgE$^+$ cells. *Nat. Immunol.* 13:623, author reply : 623–624. http://dx.doi.org/10.1038/ni.2313

Lam, K.P., R. Kühn, and K. Rajewsky. 1997. In vivo ablation of surface immunoglobulin on mature B cells by inducible gene targeting results in rapid cell death. *Cell*. 90:1073–1083. http://dx.doi.org/10.1016/S0092-8674(00)80373-6

Liu, Q., A.J. Oliveira-Dos-Santos, S. Mariathasan, D. Bouchard, J. Jones, R. Sarao, I. Kozieradzki, P.S. Ohashi, J.M. Penninger, and D.J. Dumont. 1998. The inositol polyphosphate 5-phosphatase ship is a crucial negative regulator of B cell antigen receptor signaling. *J. Exp. Med.* 188:1333–1342. http://dx.doi.org/10.1084/jem.188.7.1333

Lorenz, M., S. Jung, and A. Radbruch. 1995. Switch transcripts in immunoglobulin class switching. *Science*. 267:1825–1828. http://dx.doi.org/10.1126/science.7892607

Luger, E.O., V. Fokuhl, M. Wegmann, M. Abram, K. Tillack, G. Achatz, R.A. Manz, M. Worm, A. Radbruch, and H. Renz. 2009. Induction of long-lived allergen-specific plasma cells by mucosal allergen challenge. *J. Allergy Clin. Immunol.* 124:819–826: e4. http://dx.doi.org/10.1016/j.jaci.2009.06.047

Mandler, R., F.D. Finkelman, A.D. Levine, and C.M. Snapper. 1993. IL-4 induction of IgE class switching by lipopolysaccharide-activated murine B cells occurs predominantly through sequential switching. *J. Immunol.* 150:407–418.

Matsuoka, M., K. Yoshida, T. Maeda, S. Usuda, and H. Sakano. 1990. Switch circular DNA formed in cytokine-treated mouse splenocytes: evidence for intramolecular DNA deletion in immunoglobulin class switching. *Cell*. 62:135–142. http://dx.doi.org/10.1016/0092-8674(90)90247-C

Meyer-Hermann, M.E., P.K. Maini, and D. Iber. 2006. An analysis of B cell selection mechanisms in germinal centers. *Math. Med. Biol.* 23:255–277. http://dx.doi.org/10.1093/imammb/dql012

Meyer-Hermann, M., E. Mohr, N. Pelletier, Y. Zhang, G.D. Victora, and K.M. Toellner. 2012. A theory of germinal center B cell selection, division, and exit. *Cell Rep.* 2:162–174. http://dx.doi.org/10.1016/j.celrep.2012.05.010

Mootha, V.K., C.M. Lindgren, K.F. Eriksson, A. Subramanian, S. Sihag, J. Lehar, P. Puigserver, E. Carlsson, M. Ridderstråle, E. Laurila, et al. 2003. PGC-1alpha-responsive genes involved in oxidative phosphorylation are coordinately downregulated in human diabetes. *Nat. Genet.* 34:267–273. http://dx.doi.org/10.1038/ng1180

Okada, H., S. Bolland, A. Hashimoto, M. Kurosaki, Y. Kabuyama, M. Iino, J.V. Ravetch, and T. Kurosaki. 1998. Role of the inositol phosphatase SHIP in B cell receptor-induced Ca2+ oscillatory response. *J. Immunol.* 161:5129–5132.

Pani, G., M. Kozlowski, J.C. Cambier, G.B. Mills, and K.A. Siminovitch. 1995. Identification of the tyrosine phosphatase PTP1C as a B cell antigen receptor-associated protein involved in the regulation of B cell signaling. *J. Exp. Med.* 181:2077–2084. http://dx.doi.org/10.1084/jem.181.6.2077

Pape, K.A., J.J. Taylor, R.W. Maul, P.J. Gearhart, and M.K. Jenkins. 2011. Different B cell populations mediate early and late memory during an

endogenous immune response. *Science*. 331:1203–1207. http://dx.doi.org/10.1126/science.1201730

Rabbitts, T.H., A. Forster, W. Dunnick, and D.L. Bentley. 1980. The role of gene deletion in the immunoglobulin heavy chain switch. *Nature*. 283:351–356. http://dx.doi.org/10.1038/283351a0

Saeed, A.I., V. Sharov, J. White, J. Li, W. Liang, N. Bhagabati, J. Braisted, M. Klapa, T. Currier, M. Thiagarajan, et al. 2003. TM4: a free, open-source system for microarray data management and analysis. *Biotechniques*. 34:374–378.

Siebenkotten, G., C. Esser, M. Wabl, and A. Radbruch. 1992. The murine IgG1/IgE class switch program. *Eur. J. Immunol*. 22:1827–1834. http://dx.doi.org/10.1002/eji.1830220723

Smith, K.G., U. Weiss, K. Rajewsky, G.J. Nossal, and D.M. Tarlinton. 1994. Bcl-2 increases memory B cell recruitment but does not perturb selection in germinal centers. *Immunity*. 1:803–813. http://dx.doi.org/10.1016/S1074-7613(94)80022-7

Smith, K.G., A. Light, L.A. O'Reilly, S.M. Ang, A. Strasser, and D. Tarlinton. 2000. bcl-2 transgene expression inhibits apoptosis in the germinal center and reveals differences in the selection of memory B cells and bone marrow antibody-forming cells. *J. Exp. Med*. 191:475–484. http://dx.doi.org/10.1084/jem.191.3.475

Smyth, G.K. 2004. Linear models and empirical bayes methods for assessing differential expression in microarray experiments. *Stat. Appl. Genet. Mol. Biol*. 3:e3.

Subramanian, A., P. Tamayo, V.K. Mootha, S. Mukherjee, B.L. Ebert, M.A. Gillette, A. Paulovich, S.L. Pomeroy, T.R. Golub, E.S. Lander, and J.P. Mesirov. 2005. Gene set enrichment analysis: a knowledge-based approach for interpreting genome-wide expression profiles. *Proc. Natl. Acad. Sci. USA*. 102:15545–15550. http://dx.doi.org/10.1073/pnas.0506580102

Talay, O., D. Yan, H.D. Brightbill, E.E. Straney, M. Zhou, E. Ladi, W.P. Lee, J.G. Egen, C.D. Austin, M. Xu, and L.C. Wu. 2012. IgE^+ memory B cells and plasma cells generated through a germinal-center pathway. *Nat. Immunol*. 13:396–404. http://dx.doi.org/10.1038/ni.2256

Tarlinton, D.M., and K.G. Smith. 2000. Dissecting affinity maturation: a model explaining selection of antibody-forming cells and memory B cells in the germinal centre. *Immunol. Today*. 21:436–441. http://dx.doi.org/10.1016/S0167-5699(00)01687-X

Thaunat, O., A.G. Granja, P. Barral, A. Filby, B. Montaner, L. Collinson, N. Martinez-Martin, N.E. Harwood, A. Bruckbauer, and F.D. Batista. 2012. Asymmetric segregation of polarized antigen on B cell division shapes presentation capacity. *Science*. 335:475–479. http://dx.doi.org/10.1126/science.1214100

Urban, J.F. Jr., K.B. Madden, A. Svetić, A. Cheever, P.P. Trotta, W.C. Gause, I.M. Katona, and F.D. Finkelman. 1992. The importance of Th2 cytokines in protective immunity to nematodes. *Immunol. Rev.* 127:205–220. http://dx.doi.org/10.1111/j.1600-065X.1992.tb01415.x

Vascotto, F., D. Le Roux, D. Lankar, G. Faure-André, P. Vargas, P. Guermonprez, and A.M. Lennon-Duménil. 2007. Antigen presentation by B lymphocytes: how receptor signaling directs membrane trafficking. *Curr. Opin. Immunol*. 19:93–98. http://dx.doi.org/10.1016/j.coi.2006.11.011

Victora, G.D., and M.C. Nussenzweig. 2012. Germinal centers. *Annu. Rev. Immunol*. 30:429–457. http://dx.doi.org/10.1146/annurev-immunol-020711-075032

Victora, G.D., T.A. Schwickert, D.R. Fooksman, A.O. Kamphorst, M. Meyer-Hermann, M.L. Dustin, and M.C. Nussenzweig. 2010. Germinal center dynamics revealed by multiphoton microscopy with a photoactivatable fluorescent reporter. *Cell*. 143:592–605. http://dx.doi.org/10.1016/j.cell.2010.10.032

Victora, G.D., D. Dominguez-Sola, A.B. Holmes, S. Deroubaix, R. Dalla-Favera, and M.C. Nussenzweig. 2012. Identification of human germinal center light and dark zone cells and their relationship to human B-cell lymphomas. *Blood*. 120:2240–2248. http://dx.doi.org/10.1182/blood-2012-03-415380

Vieira, P., and K. Rajewsky. 1988. The half-lives of serum immunoglobulins in adult mice. *Eur. J. Immunol*. 18:313–316. http://dx.doi.org/10.1002/eji.1830180221

Wesemann, D.R., A.J. Portuguese, J.M. Magee, M.P. Gallagher, X. Zhou, R.A. Panchakshari, and F.W. Alt. 2012. Reprogramming IgH isotype-switched B cells to functional-grade induced pluripotent stem cells. *Proc. Natl. Acad. Sci. USA*. 109:13745–13750. http://dx.doi.org/10.1073/pnas.1210286109

Xiong, H., M.A. Curotto de Lafaille, and J.J. Lafaille. 2012a. What is unique about the IgE response? *Adv. Immunol*. 116:113–141. http://dx.doi.org/10.1016/B978-0-12-394300-2.00004-1

Xiong, H., J. Dolpady, M. Wabl, M.A. Curotto de Lafaille, and J.J. Lafaille. 2012b. Sequential class switching is required for the generation of high affinity IgE antibodies. *J. Exp. Med*. 209:353–364. http://dx.doi.org/10.1084/jem.20111941

Yang, Z., B.M. Sullivan, and C.D. Allen. 2012. Fluorescent in vivo detection reveals that IgE(+) B cells are restrained by an intrinsic cell fate predisposition. *Immunity*. 36:857–872. http://dx.doi.org/10.1016/j.immuni.2012.02.009

Yoshida, K., M. Matsuoka, S. Usuda, A. Mori, K. Ishizaka, and H. Sakano. 1990. Immunoglobulin switch circular DNA in the mouse infected with Nippostrongylus brasiliensis: evidence for successive class switching from mu to epsilon via gamma 1. *Proc. Natl. Acad. Sci. USA*. 87:7829–7833. http://dx.doi.org/10.1073/pnas.87.20.7829

Zhang, K., F.C. Mills, and A. Saxon. 1994. Switch circles from IL-4-directed epsilon class switching from human B lymphocytes. Evidence for direct, sequential, and multiple step sequential switch from mu to epsilon Ig heavy chain gene. *J. Immunol*. 152:3427–3435.

Zhang, Y., M. Meyer-Hermann, L.A. George, M.T. Figge, M. Khan, M. Goodall, S.P. Young, A. Reynolds, F. Falciani, A. Waisman, et al. 2013. Germinal center B cells govern their own fate via antibody feedback. *J. Exp. Med*. 210:457–464. http://dx.doi.org/10.1084/jem.20120150